Late Cretaceous felsic intrusions in oceanic plateau basalts in SW Ecuador: Markers of subduction initiation?

M. Seyler, C. Witt, B. Omaña, C. Durand, M. Chiaradia, D. Villagomez, Marc Poujol

Late Cretaceous felsic intrusions in oceanic plateau basalts in SW Ecuador: markers of subduction initiation?

Seyler, M.,[1], Witt, C.[1], Omaña, B.[1], Durand, C.[2], Chiaradia, M.[3], Villagomez, D.[4], Poujol, M[5].

1 : Univ. Lille, CNRS, Univ. Littoral Côte d'Opale, UMR 8187, LOG, Laboratoire d'Océanologie et de Géosciences, F 59000 Lille, France

2 : Univ. Lille, IMT Lille Douai, Univ. Artois, Yncrea Hauts-de-France, ULR 4515 - LGCgE, Laboratoire de Génie Civil et géo-Environnement, F-59000 Lille, France.

3 : Department of Mineralogy, University of Geneva.

4 : Tectonic Analysist

5 : Univ. Rennes, CNRS, Géosciences Rennes - UMR 6118, F-35000 Rennes, France

Corresponding author.

E-mail adress: cesar.witt@univ-lille.fr (César Witt)

Key words: Caribbean oceanic plateau, tonalite, subduction initiation, SW Ecuador

Abstract

Felsic magmatic rocks (tonalites and trondhjemites) with calc-alkaline affinity were emplaced in SW Ecuador (Pascuales area; North Guayaquil) at ~87–89 Ma intruding the top

of the basalts of the Caribean Large Igneous Province (CLIP), prior to the development of typical well-known island arcs from ~85-80 Ma onwards. A clear depletion of REE distinguishes the Pascuales felsic rocks from the more differentiated lavas of the Rio Cala Arc in Ecuador and from other Late Cretaceous arc-like felsic intrusives emplaced within the CLIP in Colombia and the Antilles. In addition, the Pascuales tonalites have very low K_2O (< 0.4 wt.%), TiO_2 (< 0.4 wt.%) and P_2O_5 (< 0.15 wt.%) contents compared to dacitic rocks of the Rio Cala Arc. In contrast, their geochemistry and their similar age suggest that the Pascuales tonalites are an equivalent of the Las Orquideas dacitic volcanic rocks. The Pascuales felsic rocks have the less radiogenic Nd compositions of the whole spectrum of Ecuadorian oceanic plateau rocks, nevertheless shearing similarities with some Totoras amphibolites. The geochemical characteristics of the Pascuales intrusives and Las Orquideas dacites are similar to those formed by hydrous partial melting of mafic protoliths. The dacitic magmas must have been in equilibrium with residual mineral assemblages largely dominated by amphibole + Fe–Ti oxides (no garnet). This requires two conditions: 1) low-pressure melting under high water content and 2) a source rock extremely depleted in minor incompatible elements (K, Ti, P, Y) and REE. These conditions are fulfilled by partial melting of mafic-ultramafic cumulates undergoing high temperature and shear deformation at the base of the oceanic plateau triggered by new basaltic intrusions. The Pascuales felsic rocks emplaced at the SW border of the oceanic plateau during its final stage of building; they can thus be related to asthenopheric upwelling during the initial stage of island arc magmatism.

1. Introduction

The Caribbean Large Igneous Province (CLIP; Fig. 1) is an oceanic terrane currently exposed in the Caribbean region and in northwestern South America. The CLIP mainly

extruded between 100 Ma and 88 Ma (e.g. Kerr et al., 2003; Luzieux et al., 2006; Sinton et al., 1998; Villagómez et al., 2011; Wattam and Stern, 2015), although significantly younger rocks up to circa 65 Ma have been observed in the Gorgona Island and Western Colombia (Serrano et al., 2011; Sinton et al., 1998). The origin of the CLIP is also debated with theories proposing an extrusion in a location close to the paleo-Galapagos hot spot (e.g. Duncan et al., 1984; Whattam and Stern, 2015) or an origin related to a different plume event (e.g. Boschman et al., 2014). The borders of the CLIP are characterized by plateau basaltic rocks and tonalitic magmatism, the latter being ascribed to the melting of the plateau or to incipient subduction processes (e.g. White et al., 1999; Wright and Wyld, 2011; Villagomez et al., 2011; Whattam and Stern, 2015; Weber et al., 2015). Because of its high buoyancy and thickness (between 8 and >20 km; Kerr et al., 2003) it is believed that the CLIP (and an associated island arc) accreted to the South American margin between 80 Ma and 65 Ma (Vallejo et al., 2009; Villagómez et al., 2011; Kerr et al., 2002a; Hughes and Pilatasig, 2002; Jaillard et al., 2009).

Rocks from the southern limit of the CLIP in SW Ecuador include: 1) basalts, dolerites and gabbros typical of plateau settings with ages ranging between 90 Ma and 85 Ma (Kerr et al., 2002a; Luzieux et al., 2006; Vallejo et al., 2009, 2006), an interval that coincides with the major pulse of CLIP magmatic activity and with the supposed plume-induced subduction initiation at the margins of the CLIP, and 2) Late Cretaceous intrusive and volcanoclastic deposits (with ages also roughly coincident with the suggested subduction initiation beneath the CLIP) that have geochemical affinities that may relate them to a juvenile subduction setting (see also the bachelors thesis of Macias, 2018). However, various works in southwest and central Ecuador (Allibon et al., 2008; Amórtegui et al., 2011; van Melle et al., 2008) suggest that similar geochemical characteristics may result from the partial melting of the base of the oceanic plateau. Farther north, in the Western Cordillera of Ecuador, La Portada

Unit assigned to the base of the Rio Cala island arc (Kerr et al., 2002a; van Thournout, 1991; Wilkinson, 1998) and the Pujilí Granite (PG in Fig. 2) have been ascribed to the oldest evidences of subduction beneath the CLIP in Ecuador at ~85 Ma (Vallejo, 2007; Vallejo et al., 2009).

In the SW Ecuadorian forearc region, the CLIP rocks crop out at the Chongón-Colonche Hills (CCH, Figs. 1 and 2). The CCH hills are defined by a major positive gravimetric anomaly probably related to crustal thinning (the crust is only ~7 km thick versus ~15 km in average in the forearc) and resulting mantle upwelling (Aizprua et al., 2020). Several small tonalitic, gabbroic and ultramafic bodies intrude the CLIP rocks close to the area where the CCH is buried westwards beneath the Plio-Quaternary sedimentary cover (Fig. 2; Pichler and Aly, 1983; Benitez, 1995; Eguez et al., 2017). These intrusions were poorly studied in the past and, in addition, most outcrops are now extensively covered by new civil constructions. Tonalitic intrusive bodies located near the town of Pascuales (Fig. 3A) have reported K-Ar ages of 73.3 ± 4.8 Ma (Pichler and Aly, 1983) similarly to other circa K-Ar 70 Ma cooling ages that can be arguably interpreted as a thermal cooling event related to the collision of the CLIP onto South America (e.g. Aspden and Litherland, 1992). To date, there are no published geochemical nor geochronologic constrains for the intrusive rocks located near the town of Pascuales, which is unfortunate because they might help unravel part of the youngest Cretaceous geodynamic processes that occurred in SW Ecuador. In this work we present the results of in situ LA-ICP-MS U-Pb dating on zircon and new petrographic, geochemical and isotopic analyses on felsic intrusions sampled near Pascuales (Fig. 3A), as well as new geochemical and isotopic whole rock analyses on the country basaltic rocks. These data allow us to chemically characterize a group of intermediate to felsic magmatic rocks with calc-alkaline affinity, which emplaced at ~87–89 Ma at the top of the CLIP basalts (i.e. prior to the development of Late Cretaceous island arcs). In this context, the new data

presented here is combined with previously published analyses for plateau and island arc suites in Ecuador (i.e., Las Orquideas Member, Rio Cala Arc, San Lorenzo Formation) and Colombia in order to discuss the possible origins of these arc-like rocks, as well as their relations with the country-rock oceanic plateau basalts and resulting geodynamic implications.

2. Geological context

The Andean chain in Ecuador shows two distinctive Eastern and Western Cordilleras in which topographic growth most likely took place during the last 75-70 Ma (Gutiérrez et al., 2019; Spikings et al., 2010; Witt et al., 2017). The basement of the forearc and Western Cordillera (WC) is made up of oceanic plateau basalts (herein referred as OPB) which were accreted to the continental margin of South America. These accreted terrains have been ascribed to the Piñón, Pallatanga, San Juan and Guaranda terranes, units or formations (Fig. 2; Hughes and Pilatasig, 2002; Jaillard et al., 2009; Kerr et al., 2002a; Mamberti el al., 2003; Vallejo et al., 2009). The definition of the nature, number and timing of accretion events has been one of the most debated topics in the Ecuadorian geology for the last 30 years. For some authors, a single Caribbean type accretion occurred between 75-65 Ma (Luzieux et al., 2006; Vallejo et al., 2009; Chiaradia, 2009) whereas other studies suggest multi-episodic oceanic accretions (some of them with no Caribbean affinities) at ~75 Ma, ~68 Ma and ~58 Ma, and even early Eocene (e.g. Feininger, 1987; Hughes and Pilatasig, 2002; Jaillard et al., 2009; Kerr et al., 2002a; Aizprua et al., 2019). The debate is mostly originated by differences in the subduction polarity and the age of some oceanic rocks ascribed to the San Juan Formation (see below). Accretional events are believed to represent one of the main driving factors for the generation of relief in the Ecuadorian Andes (Jaillard et al., 2009; Witt et al., 2017).

The Piñón Formation (Fm.) represents the mafic plume-related basement of the Ecuadorian forearc and is mainly composed of tholeiitic, massive and pillowed basaltic and basalt–andesitic lavas, locally intruded by dolerites and/or gabbroic stocks (e.g. Kerr et al., 2003; Reynaud et al., 1999). In the CCH, the top of the Piñón Fm. has been ascribed to the lower part of the Coniacian (i.e. ~90 Ma) based on planktic foraminifera and radiolarians collected in cherts intercalated between pillow lavas and on the age of the overlying Calentura Fm. (Ordoñez et al, 2006; van Melle et al., 2008; Velasco and Mendoza, 2003). Furthermore, a gabbro within the Piñón Fm. yielded a hornblende $^{40}Ar/^{39}Ar$ plateau age of 88.8 ± 1.6 Ma (Luzieux et al., 2006). The CCH is defined by one of the most significant gravimetric positive anomalies in the Northern Andes which most likely resulted from significant crustal thinning (the crust is only ~7 km thick in the CCH) and related denudation and mantle upwelling (Aizprua et al., 2020).

In the Western Cordillera, the Pallatanga / Guaranda Unit (92–88 Ma, Fig. 2; Kerr et al., 2002b; Kerr et al., 2003), likely also a fragment of the CLIP, is petrographically and geochemically similar to the Piñón basalts and dolerites (Kerr et al., 2002a; Mamberti et al., 2003). To the east of the Western Cordillera (Fig. 2), cumulate peridotites and gabbros intruded by mafic and felsic dykes of the San Juan Unit crop out as tectonic slices entrained within the Late Cretaceous ocean-continent suture (Hughes and Bermudez, 1997; Fig. 2). This unit is either interpreted as the root of the Pallatanga Unit (Lapierre et al., 2000; Hughes and Pilatasig, 2002) or as a magmatic chamber within the oceanic plateau (Mamberti et al., 2004). A gabbro of the San Juan Unit (SJG in Fig. 2) yielded a zircon U-Pb age of 87.1 ± 1.6 Ma interpreted as the crystallization age (Vallejo et al., 2006), comparable to the 88.8 ± 1.6 Ma $^{40}Ar/^{39}Ar$ age obtained from the Piñón hornblende gabbro by Luzieux et al. (2006). Similarly, in the Tortoras area (TA in Fig. 2) one amphibolite yielded an age of 84.7 ± 2.2 Ma ($^{40}Ar/^{39}Ar$ in hornblende interpreted as a cooling age following amphibolite facies metamorphism prior

148 to the accretion of the oceanic plateau (Vallejo et al., 2006). However, an age obtained from
149 gabbroic units also ascribed to the San Juan unit yielded a Sm/Nd isochron of 123±13 Ma
150 (Lapierre et al., 2000); suggesting that these rocks represent an older eruptive phase of the
151 plateau and most likely an older accretionary process. Indeed, Miocene transpressive faults
152 crosscutting the Western Cordillera also exhumed mafic granulites and amphibolites with
153 geochemical and Nd isotopic compositions characteristic of oceanic plateau basalts (Jaillard
154 et al., 2004; Beaudon et al., 2005; Amortegui et al., 2011), which differ from the Pallatanga
155 Unit and Piñón Fm. because they have Pb isotopic features similar to those of the Late
156 Cretaceous intra-oceanic arc (Amortegui et al., 2011).

157 In SW Ecuador, the Piñon Fm. is mostly overlain by magmatic or volcanoclastic
158 successions with island arc affinities ascribed to the Santonian Cayo and Campanian-
159 Maastrichtian San Lorenzo Fms., the latest cropping out at the NE directed Coastal Cordillera
160 (Lebrat et al., 1987; Luzieux et al., 2006; van Melle et al., 2008; Reynaud et al., 1999; Figs. 1
161 and 2). However, in the CCH to the west of Guayaquil, a thin layer of volcanic rocks referred
162 to as the Las Orquideas (LO) Member is intercalated between the Piñon basalts and the
163 Calentura and Cayo sedimentary and volcaniclastic deposits (Reynaud et al., 1999; van Melle
164 et al., 2008). The LO Member is a 30 to 150 m thick lava sequences mainly composed of
165 explosive, intermediate to dacitic products (Benitez, 1995; Reynaud et al., 1999; van Melle et
166 al., 2008). Pelagic microfauna in interbedded limestones allowed attribution of the LO
167 volcanism to the Middle Coniacian (~88 Ma; van Melle et al., 2008 and references therein).
168 Despite the calc-alkaline signature of the LO rocks, van Melle et al. (2008) considered that
169 their emplacement in a subduction setting was very unlikely mainly because the generation of
170 arc magma at ~ 100 km depth and its ascent to the surface would require more than the
171 observed ~2 Ma time interval between the end of plume activity and the eventual formation of
172 the subduction zone (i.e. with respect to the 85 Ma Pujili granite). Furthermore, these authors

suggested that the small volume of the volcanic cover is atypical for an island arc setting. Instead, these authors proposed that the LO volcanic rocks were generated by partial melting of deep parts of the CLIP.

In the Western Cordillera, arc sequences developed on top of the oceanic plateau (Fig. 2), both before and after their accretion(s) onto the continent. The Rio Cala Group (Santonian to early Maastrichtian; Hughes and Bermúdez, 1997; Boland et al., 2000) and its tholeiitic Rio Cala island arc (66.7 ± 7.2 Ma Ma, Vallejo et al., 2009) represents the oldest clear evidence of arc magmatism observed in the Western Cordillera, yet its original position may have been related to either westwards (e.g. Vallejo et al., 2009) or eastward (e.g. Jaillard et al., 2009) subduction prior to the main accretional period 75-65 Ma ago (Vallejo et al., 2009; Chiaradia, 2009). An older age of 85.5 ± 1.4 Ma (zircon LA-ICP-MS U-Pb age; Vallejo et al., 2006) was obtained for the Pujilí Granite, which occurs within a tectonic block within the continent - ocean suture, east of the Western Cordillera (PG in Fig. 2). The adakitic nature of the Pujilí Granite and some plume-like mineralogical and geochemical characteristics of the Late Cretaceous arc magmatism in SW Ecuador suggest a hot subduction zone, which possibly facilitated the incorporation of a mantle plume component in the arc magmas through assimilation and/or partial melting of the CLIP (Allibon et al., 2008; Vallejo et al., 2009). According to Whattam and Stern (2015), all Late Cretaceous magmatic events (i.e. post-100 Ma) in Southern Ecuador correspond to hybrid magmas with both plume and subduction zone contributions, with a progressive increasing amount of subduction-related magma in the hybrid plume-mantle source.

3. Sampling and analytical methods

Samples of this study were collected north of Guayaquil in the easternmost border of the CCH (Fig. 2), near the town of Pascuales (Fig. 3A) where intrusions of felsic plutonic rocks occur within ~2-4 km long ~ 1.5 km wide areas (red outlines in Fig. 3A). The best two preserved outcrops show subhorizontal, ~5 m thick, layers of massive, greenish to grey pale rocks affected by numerous orthogonal fractures. One of the outcrops (Fig. 3B) provided two pieces of trondhjemites (GD001 and GD002) forming the lower layer, while three tonalite pieces were sampled in the upper layer (GD003, CP601, CP024). A fourth trondhjemitic sample (CP603) was collected in the second outcrop (Fig. 3C). Rocks surrounding the felsic intrusions are medium to fine grained basalts and metabasalts showing variable degrees of mylonitization and alteration. Locally, they are cross-cut by hornblende-filled shear zones, and veinlets or microdykes composed of dioritic mineral assemblages (plagioclase, magnesiohornblende and opaque minerals). Least altered volcanic mafic rocks were also sampled at different locations (CP605, CP607, GD004; Fig. 3A). Mineral compositions of selected samples were determined with a CAMECA SX100 electron microprobe with 4 wavelength-dispersive spectrometers at the Ecole Nationale Supérieure de Chimie in Lille University. Analytical conditions were 15 kV acceleration voltage, 15nA beam current and a peak counting time of 20s. Natural standards were used for the electron microprobe calibration. Zircon U-Pb geochronology was conducted by in-situ laser ablation inductively coupled plasma mass spectrometry (LA-ICP-MS) at the GeOHeLiS analytical platform (Géosciences Rennes/OSUR, Univ. Rennes) using an ESI NWR193UC Excimer laser coupled to a quadrupole Agilent 7700x ICP-MS equipped with a dual pumping system to enhance sensitivity. Concordia ages and diagrams were generated using Isoplot/Ex (Ludwig, 2012). Operating conditions are presented in Table S1. For a more detailed description of the analytical protocol see Manzotti et al. (2015) and Witt et al. (2019). Whole-rock compositions

were obtained by fusion technique (lithium metaborate/tetraborate). Diluted solutions were analyzed for major oxides by Inductively-Coupled Plasma Optical Emission Spectrometry (ICP-OES) and by Inductively-Coupled Plasma Mass Spectrometry (ICP-MS) for trace elements, at the Actlabs laboratory (Ontario, Canada) according to code 4Lithoresearch package. The international standards used for analytical control were BIR-1a (basalt), DCN-1 (dolerite), GBW 07113 (rhyolite), TDB-1 (diabase rock), DTS-2b (dunite), SY-4 (diorite gneiss), NCS DC86312 (rare earth ore) CTA-AC-1 (apatite concentrate). for further details, see http://ww.actlabs.com.

Radiogenic isotope ratios of Sr ($^{87}Sr/^{86}Sr$), Nd ($^{143}Nd/^{144}Nd$) and Pb ($^{206}Pb/^{204}Pb$, $^{207}Pb/^{204}Pb$, $^{208}Pb/^{204}Pb$) were measured at the Department of Earth Sciences (University of Geneva, Switzerland). The method is described in detail in Chiaradia et al. (2020). Briefly, 100 to 120 mg of whole rock powder were dissolved in concentrated HF and HNO_3. Samples were dried and re-dissolved in concentrated HNO_3 and dried again. Sr, Nd and Pb were then separated using cascade columns with Sr-Spec, TRU-Spec and Ln-Spec resins according to a protocol modified from Pin et al. (1994). The material was finally redissolved in 2% HNO_3 solutions and ratios were measured using a Thermo Neptune PLUS Multi-Collector ICP-MS in static mode. Long-term (>2 years) reproducibility of SRM987 (McArthur et al., 2001), JNdi-1 (Tanaka et al., 2000) and SRM981 (Baker et al., 2004) standards are 10 ppm (1SD) for 87Sr/86Sr and 143Nd/144Nd, 0.0048% for $^{206}Pb/^{204}Pb$, 0.0049% for $^{207}Pb/^{204}Pb$ and 0.0062% for $^{208}Pb/^{204}Pb$. $^{87}Sr/^{86}Sr$, $^{143}Nd/^{144}Nd$ and Pb isotope ratios were corrected for external fractionation (due to a systematic difference between measured and accepted standard ratios) by a value of -0.021‰, +0.051‰ and +0.36‰ amu respectively. Total procedural blanks were <500 pg for Pb and <100 pg for Sr and Nd which are insignificant compared to the amounts of these elements purified from the whole rock samples investigated.

4. Petrography and mineralogy

4.1. Felsic rocks

Samples CP601, CP024, GD003 are medium-grained tonalites composed of quartz (~27–32 vol.%), plagioclase (~50–55 vol.%) and green amphibole (~10–12 vol.%; supplementary Fig. S1A). Plagioclase and amphibole occur as euhedral-subhedral prismatic crystals, while quartz is mainly present in a granular mosaic texture enclosing the former minerals. Apatite, titanite, zircon and titanomagnetite are accessory minerals. Plagioclase grains are zoned with Ca-rich cores and Na-rich rims; their compositions range from $An_{55}Ab_{44}Or_{1}$ to $An_{7}Ab_{88}Or_{4}$ (average $An_{39.6}Ab_{59.0}Or_{1.4}$; n = 27). Dark green magnesiohornblende forms stubby, commonly twinned, prismatic crystals, locally replaced by actinolite. Minor amounts of epidote, chlorite and magnetite also occur as intergranular phases and as inclusions in the magnesiohornblende cores where they may represent former pyroxenes. Samples CP603 (Fig. S1B), GD001 and GD002 mostly consist of euhedral-subhedral albite ($Ab_{99\pm1}$; n = 17) and quartz in near equal amounts, and correspond to trondhjemites following the definition of Barker (1979). Textures are hipidiomorphic granular to granophyric (e.g., graphic intergrowths of quartz and albite forming almost 20 vol.% of the rocks). Primary mafic minerals (up to 7 vol.%, likely former amphiboles) are replaced by chlorite, Fe-oxides and epidote group minerals. Titanomagnetite ± ilmenite, titanite and zircon occur as accessory phases.

4.2. Mafic rocks

271

272 *4.2.1 Petrography*

273

274 Sample CP605 (Fig. S1C) is a dark green, fine-grained, undeformed and homogeneous
275 metabasite. Rare, euhedral to subhedral, clinopyroxene phenocrysts (400–600 µm in diameter;
276 ~1 vol.%) are fully pseudomorphosed by green amphiboles. Groundmass is intersertal-
277 intergranular, composed of skeletal plagioclase laths ($An_{41\pm11}$; n = 38), clinopyroxene grains
278 partially replaced by amphibole, and accessory ilmenite, titanomagnetite, apatite and pyrite.
279 Sheaf-like radial clusters of plagioclase are also observed. Low-grade secondary minerals
280 form less than 5 vol.% and are represented by chlorite, albite, epidote, titanite, biotite and
281 magnetite. Sample CP607 (Fig. S1D) shows a cataclastic structure but has preserved
282 undeformed parts with igneous texture that are large enough to be analyzed. Igneous texture is
283 sparsely phyric (<1 vol.%) with ~1–2 mm sized, subhedral pseudomorphs of clinopyroxene
284 phenocrysts fully replaced by brownish to dark green amphiboles. They have spongy cores
285 enclosing groundmass and are surrounded by ~100 µm - thick corona also replaced by
286 amphiboles whose shapes and color are similar to those in the cores but oriented differently.
287 Groundmass is holocrystalline, medium-grained (400–600 µm), made of plagioclase laths
288 partially albitized and clinopyroxenes replaced by amphibole, titanite and magnetite.
289 Accessory ilmenite and titanomagnetite are widespread in groundmass. Other low-grade
290 secondary minerals (< 5 vol.%) are albite, chlorite, magnetite, quartz, epidote group minerals
291 and biotite. Sample GD004 (Fig. S1E) is a medium-grained (200–700 µm), isogranular basalt
292 made of plagioclase, clinopyroxene and abundant, up to 150 µm sized crystals of ilmenite and
293 titanomagnetite. Hydrothermal alteration is marked by replacement of plagioclase, pyroxene
294 and Fe-Ti oxides by albite, diopside, epidote, titanite and crystallization of pyrite-
295 chalcopyrite.

296

297 *4.2.2. Mineral chemistry*

298

299 Fresh clinopyroxenes (Table S2; Fig. 4A,B) have been only preserved in samples
300 CP605 and GD004. In CP605 they are magnesian augites ($En_{49.7\pm0.9}Wo_{39.4\pm0.9}Fs_{11.0\pm0.8}$; n = 16)
301 which show variable Al_2O_3 contents (2.21 ± 0.36 wt.%) negatively correlated with Mg# [=
302 molar Mg/(Mg + Fe_{tot}) = 83–80]. Although somewhat scattered, GD004 clinopyroxenes are
303 augites ($En_{48.0\pm0.5}Wo_{37.1\pm0.6}Fs_{14.9\pm0.7}$; Mg# 78–75; n = 36) slightly poorer in Al_2O_3 (1.93 ± 0.14
304 wt.%).

305 Primary plagioclase compositions range from An_{59} to An_{24} ($An_{42\pm11}$; n=47) in CP605
306 and from An_{75} to An_{25} ($An_{51\pm16}$; n = 48) in CP607. In both samples secondary albitic
307 compositions ($An_{9\pm3}$ in CP605; $An_{10\pm2}$ in CP607) forming 12–15% of the analytical set are
308 separated from the primary compositions by a compositional gap. In GD004 all the
309 plagioclases are albitized.

310 Amphiboles are the major mafic phases in CP605 and CP607 and are absent in
311 GD004. Their compositions calculated according to the 13-cations method (e.g. Leake et al.,
312 1997; Ridolfi et al., 2010) are listed (Table S2). They are Ti-poor (Ti ≤ 0.1 apfu), Mg-rich
313 [Mg/(Mg + Fe^{2+}) = 0.6–0.8] calcic ($[Ca]_B$ = 1.7–1.9 apfu) amphiboles showing a large range
314 of compositions (Fig. 4C). Aluminous end-member compositions (^{IV}Al = 1.6–2.0 and [Na +
315 $K]_A$ = 0.46–0.58) occur as small, relic inclusions within the less aluminous amphiboles (Fig.
316 S1F). Their compositions are transitional between tschermakitic pargasite ($^{IV}Al \geq 0.5$; [Na +
317 $K]_A < 0.5$) and magnesiohastingsite ($^{IV}Al \geq 1.5$; $[Na + K]_A \geq 0.5$) (Fig. 4D), indicating
318 crystallization at high temperature (e.g., ≥ 850 °C, Ridolfi et al., 2010 and therein references).
319 Their low Ti contents suggest a metamorphic / hydrothermal origin (e.g. Coogan et al., 2001;

320 Gillis et al., 2001, Ridolfi and Renzulli, 2012 for a review). Furthermore, a small amount of
321 chlorine was detected with the EDS (energy dispersive spectroscopy). Compositions of the
322 other amphiboles vary from magnesiohornblende to actinolitic hornblende. In both samples,
323 the wide compositional range, with decreasing ^{IV}Al (down to 0.5) positively correlated with
324 decreasing alkali contents ($[Na + K]_A$ down to 0.02) (Fig. 4D), reflect crystallization at
325 decreasing temperatures in lower to upper amphibolite facies conditions (~850–450°C,
326 Anderson and Smith, 1995; Gillis and Roberts, 1999; Helz, 1982). Replacement of the
327 pyroxenes thus started at high temperature under static conditions, likely reflecting
328 seawater/hydrothermal alteration/metamorphism that occurred shortly after eruption, when
329 the basalts were still hot. Amphiboles in veins crosscutting the basalts and associated with
330 cataclasis are low-Al hornblende and actinolite.

331

332 **5. U–Pb dating of zircon**

333

334 Two tonalites (CP024 and CP601) and one trondhjemite (CP603) were selected for U-
335 Pb dating. Results are reported in Table S3 and plotted in Fig. 5. Zircons vary from irregular
336 with few developed faces to anhedral (Fig. S1G). They show little or no
337 cathodoluminescence. For sample CP024, 18 analyses were performed on 18 different zircon
338 grains. Plotted in a Tera-Wasserburg diagram (Fig. 5A), fifteen of them are concordant within
339 error (plain line ellipses in Fig. 5A and in bold in Table S3) while three have a discordancy
340 between 5 and 9% (dashed-line ellipses in Fig. 5A). These fifteen concordant data yield a
341 concordia date (as of Ludwig, 1998) of 89.6 ± 2.0 Ma (MSWD = 1.2) identical within error
342 with the $^{206}Pb/^{238}U$ weighted date of 89.7 ± 0.6 Ma (MSWD = 0.75; n = 6). The position of
343 the three remaining discordant analyses is attributed to the presence of a slight common Pb
344 component together with a very small Pb loss (at least for analyses 25120314 and 30120314,

345 see Table S3 and Fig. 5A). Sample CP601 was collected on the same outcrop as sample
346 CP024. In this case all the seventeen analyses are discordant (Fig. 5B). This discordancy is
347 interpreted as the sign for the presence of initial (common) Pb in the analyzed zircon grains. If
348 an isochron is anchored to a $^{207}Pb/^{206}Pb$ initial value of 0.84 (calculated following then Stacey
349 and Kramers (1975) Pb evolution model for an age of 90 Ma), the resulting lower intercept
350 yields a date of 87.2 ± 1.3 Ma (MSWD = 4.6; n = 17). Thirteen zircon analyses from sample
351 CP603, plot in a concordant to discordant position (Fig. 5C) revealing different amount of
352 initial (common) Pb in the grains. Five analyses are concordant within error (grey ellipses in
353 Fig. 5C and in bold in Table S3) yield a concordia date of 86.5 ± 2.3 Ma (MSWD = 4.8; n =
354 5) while the whole set of data return a lower intercept date of 85.3 ± 1.0 Ma (MSWD = 2.2; n
355 = 13) if the isochron is anchored to a $^{207}Pb/^{206}Pb$ initial value of 0.84. In the light of these
356 data, we conclude that these felsic intrusives were emplaced 87-89 Ma ago.

357

358 **6. Elemental geochemistry**

359

360 Whole rock major element analyses were performed on five felsic and three basaltic
361 samples. Results are presented in Table 1 and plotted in Fig. 6–9 along with analyses of Late
362 Cretaceous (pre-collision) magmatic rocks from southwestern Ecuador for comparison (see
363 Fig. 2 for their spatial distributions/positions). All compositions are recalculated as volatile-
364 free and summing to 100%.

365

366 *6.1. Felsic rocks*

367

Consistent with their mineralogy, the five analyzed samples plot as tonalites (CP601 and GD003) and trondhjemites (CP603, GD001, GD002) on Barker et al. (1979)'s Ab-An-Or diagram (Fig. 6). Loss on ignition (LOI) vary from 0.85 to 1.98 wt.%, in agreement with minor hydrothermal alteration and/or weathering. The abundances in major and trace elements are plotted against silica in Figs. 7 and 8, respectively. SiO_2 contents range from 66.5–69.8 wt.% at 2.5–2.7 wt.% MgO in the tonalites to 78.0–80.1 wt.% at 0.3–0.6 wt.% MgO in the trondhjemites. The transition from tonalite to trondhjemite is marked by decreases of Fe_2O_3* (~6.3 to 1.5–3.7 wt.%), Al_2O_3 (~13.6 to 11.3 wt.%), CaO (~4.7 to 1.0 wt.%), P_2O_5 (~0.07 to 0.03 wt.%), V (127 to 12 ppm, not shown) and Sr (~216 to 64 ppm). Inversely, Na_2O (~4.1 to 5.2 wt.%), La (~4.4 to 5.6 ppm), Zr (~54 to 91 ppm), Nb (~1.7–2.2 ppm) and Th (~0.6–1.0 ppm) increase slightly. Both the tonalitic and trondhjemitic samples are characterized by extreme depletions in REE (3.7–6.2 ppm La; 0.65–0.85 ppm Yb) and Y (4.8–7.4 ppm). Compared to more differentiated lavas of the Rio Cala Arc, the Pascuales tonalites are distinctly depleted in K_2O (< 0.3 wt.%), TiO_2 (< 0.3 wt.%) and P_2O_5 (< 0.05 wt.%) contents and are 21–26% more depleted in REEs and Y at 68–70 wt% SiO_2. On the other hand, they are similar to the LO volcanic rocks having more than 57 wt.% SiO_2 (except one LO dacite which is enriched in K_2O).

Chondrite-normalized (CN) REE abundances (Fig. 9A,B) of the Pascuales felsic rocks like those of LO dacites (≥ 63 wt.% SiO_2) exhibit flat HREE concentrations (Er/Y_{CN} = ~1.0–1.1) followed by moderate enrichments in the more incompatible REE (La/Sm_{CN} = 1.5–2.0 and 1.7–2.2 in tonalite and dacite, respectively; La/Yb_{CN} 3.6–4.7 in both rock types). In contrast, the Ho/Yb_{CN} ratios in trondhjemite decrease progressively from ~1.0 in GD001 to 0.7 in GD002, together with increasing enrichments in LREE relative to MREE (La/Sm_{CN} = 2.7–4.0) and HREE (La/Yb_{CN} = 4.4–6.5); these chemical features are especially marked in the trondhjemitic sample GD002. The tonalites show moderate depletions in Eu relative to

393 adjacent REE (Eu/Eu* 0.80–0.86), while the trondhjemite GD002 displays a pronounced
394 positive Eu anomaly (Eu/Eu* = 1.43), reflecting plagioclase fractionation for the former and
395 accumulation of sodic plagioclase for the latter. The other trondhjemitic samples lack any Eu
396 anomaly.

397 On multi-element plots normalized to the Primitive Mantle (PM; Fig. 9C), all the
398 silica-rich samples display subduction-like geochemical signatures characterized by negative
399 Nb anomalies. However, Nb depletions relative to La are significantly less pronounced in the
400 Pascuales intrusives and LO dacites (Nb/La_{PM} = 0.37 ± 0.03 and 0.48 ± 0.05, respectively)
401 than in the silicic lavas from the Rio Cala Arc (Nb/La_{PM} = ~0.20 ± 0.01) and in the Pujili
402 Granite (Nb/La_{PM} = 0.10). Another major difference is the positive anomalies in Zr and Hf
403 observed in the Pascuales tonalites and LO dacites (Zr/Sm_{PM} = 1.3–1.5 and 1.5–2.8,
404 respectively) versus negative Zr and Hf anomalies in Rio Cala andesites and dacites (Zr/Sm_{PM}
405 = ~0.8 ± 0.2) and in Pujili Granite (Zr/Sm_{PM} ~0.4). In the trondhjemites, Zr and Hf spikes are
406 more pronounced (Zr/Sm_{PM} = 2.2–3.8) than in the tonalites, the trondhjemitic sample GD002
407 having the highest ratio. Plots of REE, Th, Y and Zr against Nb, a highly incompatible trace
408 element and the least mobile during hydrothermal and/or seawater alterations (Pearce, 2014),
409 show that Pascuales and LO volcanic rocks define trends with slopes intermediate between
410 those of the island arc lavas and the OPB (Fig. S2).

411 In summary, the Pascuales felsic intrusions have tonalitic and trondhjemitic
412 compositions, characterized by extremely low K_2O, TiO_2, P_2O_5 and REE concentrations; they
413 are moderately depleted in Nb relative to La and enriched in Zr and Hf relative to Sm. These
414 chemical features clearly distinguish the Pascuales felsic compositions from the silicic
415 volcanic rocks of the Rio Cala Arc, but are shared by the LO dacitic samples.

416

417 *6.2. Mafic rocks*

LOI vary from 1.6 wt% in CP605 through 2.2 wt% in CP607 to 3.9 wt% in GD004 (Table 1). On an anhydrous basis, all samples have basaltic compositions (SiO_2 = 50.8–51.7 wt%, MgO > 5 wt%). CP605 and CP607 have near primitive compositions (MgO = 7.4–8.1 wt%, Cr = 160–190 ppm, Ni = 100–110 ppm), whereas GD004 has a more differentiated composition, as shown by lower MgO (5.1 wt%), Cr (20 ppm) and Ni (40 ppm) contents and higher TiO_2, V and incompatible trace elements, such as REEs, Y, Nb, Th, Zr and Hf (Table 1).

In the Harker diagrams (Figs. 7 and 8) the three analyzed basaltic samples fall systematically within the compositional fields of the Ecuadorian OPB and, in particular, their compositions are similar to those of the Piñón basalts previously sampled in the CCH (Reynaud et al., 1999; van Melle et al., 2008). Plotted against Nb, the concentrations in alteration-mobile incompatible elements (Sr, Rb and Ba) also are within the ranges of the variably altered Ecuadorian OPB (Fig. S2). In contrast, U concentrations in CP605, and to a lesser extent in CP607, plot above the Ecuadorian OPB trend, suggesting U gain during alteration.

On a chondrite-normalized REE diagram (Fig. 9D), samples CP605 and CP607 plot in the middle of the Ecuadorian OPB field at Yb_{CN} = ~16, whereas GD004 plots at Yb_{CN} = ~29 at the upper boundary among the most evolved OPB compositions. Samples CP605 and GD004 display flat REE patterns (La/Yb_{CN} = ~0.9), while CP607 is slightly depleted in LREE (La/Yb_{CN} = ~0.6). Samples CP607 and GD004 exhibit small negative anomalies in Eu (Eu/Eu* = 0.87 and 0.93, respectively).

The Pascuales basaltic samples are significantly enriched in the most incompatible elements (Nb = 3.6–5.9 ppm, Th = 0.36–0.45 ppm) with respect to N-MORB (Fig. 9E). The values of $(Nb/La)_{N\text{-}MORB}$ (1.1–1.7) and $(Th/Nb)_{N\text{-}MORB}$ (1.5–2.1) are within the range of the

443 other Ecuadorian OPB (1.1–1.7 and 1.1–2.7, respectively) and within the range of the six
444 CCH basalts previously published (1.1–1.4 and 1.2–1.9, respectively). Nb/U ratios (12-30) are
445 lower than those in oceanic (49–50) and Ecuadorian (33–48) OPB, confirming U enrichment
446 during alteration. Sample CP607 displays a strong positive anomaly in Sr (Sr/Sr* = 2.2),
447 whereas CP605 shows a smaller positive anomaly (Sr/Sr* = 1.3), which are not correlated
448 with higher Al_2O_3 and Sr values and likely reflects alteration. In contrast, the slight Sr
449 depletion in GD004 (Sr/Sr* = 0.8) is consistent with the small Eu anomaly, indicating minor
450 plagioclase fractionation. In addition, Ti in GD004 is enriched relative to the adjacent REE,
451 reflecting Fe-Ti oxide accumulation, in agreement with high Fe_2O_3 contents and evolution
452 toward ferrobasaltic composition.

453 In summary, the basaltic rocks collected in Pascuales are tholeiites with flat to slightly
454 LREE depleted patterns, geochemically similar to the Late Cretaceous oceanic plateau basalts
455 of the Piñón Fm. Samples CP605 and CP607 have moderately differentiated compositions,
456 whereas GD004 have evolved toward a ferrobasalt, which is consistent with the mineralogy.
457 Although they crop out within a very restricted area (Fig. 3), the three basalts exhibit highly
458 variable Nb/La ratios (~1 to 1.56), suggesting that they represent different OPB units, a
459 heterogeneity typically observed in CLIP basalts (Kerr et al., 2002b, 2003).

460

461 **7. Nd, Sr and Pb isotopic data**

462

463 The three basaltic samples, one tonalite (GD003) and two trondhjemites (CP604 and
464 GD001) have been analyzed for Sr–Nd and Pb isotopic compositions. Results are reported in
465 Table 1 and plotted in Fig. 10; complete results are listed in Table S4. The basalts of this
466 study have homogeneous εNd_i (+6.9 to +7.4) similar to two (out of three) previously

published basalts from the CCH and overlap the Nd–Sr isotopic fields of the CLIP and Late Cretaceous island arc volcanic rocks from Ecuador (Fig. 10A). Relatively high $(^{87}Sr/^{86}Sr)_i$ ratios (0.70464–0.70472) are likely related to the seawater and hydrothermal alterations observed in thin sections. Nevertheless, the range of the Sr isotopic ratios for all samples is rather restricted, precluding any major alteration-induced modifications on the Sr isotopic system. The $(^{206}Pb/^{204}Pb)_i$ and $(^{207}Pb/^{204}Pb)_i$ values of the Pascuales basalts are high and slightly scattered (18.64–18.93 and 15.54–15.63, respectively) but still in the range of the Ecuadorian OPB with the exception of CP607 which has the lowest $(^{206}Pb/^{204}Pb)_i$ and the highest $(^{207}Pb/^{204}Pb)_i$ ratios (Fig. 10C). However, because of the very low values of their Nb/U ratios (12–29 versus 47 ± 10 in oceanic mantle, Hofmann, 1988), Pb isotopic data of the Pascuales basalts may not be meaningful, rather reflecting post-magmatic addition of U. Lead is also known to be mobile during alteration (Hauff et al., 2000b); but, in this study, its mobility cannot be evaluated because the concentrations are below the detection limit (<5 ppm). Pascuales felsic intrusions have relatively low εNd_i (+4.4 to +5.6), nevertheless similar to that of the CCH Piñón basalt Ca1 (+4.5) analyzed by Reynaud et al. (1999) and within the range of Late Cretaceous picrites and alkali basalts from Tortugal in Costa Rica (εNd_i = +6.9 to +4.2; Hauff et al., 2000a; Trela et al., 2017) and the Beata Ridge in the Caribbean Sea (εNd_i = +5.2–+5.4; Hauff et al., 2000b) and also similar to some gabbro–wehrlite cumulate samples from the San Juan Unit (Mamberti et al., 2004; Lapierre et al., 2010). In the diagram $(^{143}Nd/^{144}Nd)_i$ versus $(^{206}Pb/^{204}Pb)_i$ Pascuales felsic rocks fall in the same field as Tortugal lavas, which is subparallel to that of the Galapagos (Fig. 10B). The tonalite GD003 and the trondhjemite GD001, collected in the same outcrop (Fig. 3B), are similarly radiogenically enriched in $(^{206}Pb/^{204}Pb)_i$ and $(^{207}Pb/^{204}Pb)_i$ with respect to the tonalite CP603 which was sampled in a nearby outcrop (Fig. 3C) suggesting post-magmatic, small-scale variations. The more radiogenic Pb isotopes in GD001 and GD003 may reflect assimilation of minor amounts

492 of sediment which were interbedded in the basaltic crust. Small variations among the three
493 felsic rocks also affect the Sr isotopic ratios, likely in relation with late-stage hydrothermal
494 fluids.

495 In summary, the isotopic values for both Pascuales basaltic and felsic rocks are within
496 the range of Ecuadorian OPB and volcanic rocks of other parts of the Caribbean oceanic
497 plateau. However, with εNd_i ranging between +4.4 and +5.6 the felsic plutonic rocks plot
498 among the less radiogenic Nd compositions and have more radiogenic Sr and Pb
499 compositions, different from those in the host basalts, but very close to those a Piñón basalt
500 sampled in Guayaquil area. Homogeneous Nd isotopic ratios are consistent with derivation of
501 the three felsic rocks from a common source, but very limited, small-scale variability in Sr
502 and Pb isotopic composition suggests additional crustal assimilation and/or hydrothermal
503 alteration.

504

505 **8. Discussion**

506

507 *8.1 Spatial, temporal and geochemical relationships between Pascuales felsic rocks and Las*
508 *Orquideas volcanic rocks*

509

510 Both the Pascuales and LO magmatic rocks crop out in the same region of the CCH
511 west of Guayaquil. On one hand, Pascuales tonalites and trondhjemites are intrusive within
512 basalts that are similar to oceanic plateau basalts of the Piñón Fm. forming the basement of
513 the CCH (Fig. 3) in terms of major elements, trace elements, and isotopes. On the other hand,
514 LO dacites were sampled in Rio La Derecha and Rio Guaraguau located 30-40 km west from
515 Pascuales, where they conformably overlay the top of the Piñón basalts (van Melle et al.,

516 2008). The LO volcanic rocks are interbedded with limestones that contain pelagic
517 microfauna indicating a Coniacian age (Ordoñez, 2007; van Melle et al., 2008; Velasco and
518 Mendoza, 2003), i.e. corresponding to an age of ~88 Ma according to the time scale of
519 Gradstein et al. (2004). This age is consistent with the radiometric ages of 87–89 Ma obtained
520 here and interpreted as the time of crystallization of the plutonic felsic rocks, indicating that
521 the plutonic and volcanic events were coeval, or at least penecontemporaneous.

522 In addition to be closely spatially and temporally related both rock types share peculiar
523 geochemical characteristics that clearly distinguish them from Cretaceous Ecuadorian arc-
524 related volcanic rocks. Indeed, despite some scatter in K_2O, Ba, Sr (due to the mobility of
525 these elements during alteration) and in Al_2O_3, Na_2O and MgO (ascribed to variable
526 abundances of plagioclase ± pyroxene phenocrysts in the LO volcanic rocks, van Melle et al.,
527 2008; Reynaud et al., 1999), Harker diagrams (Figs. 7 and 8) and plots of REE, Th, Zr and Y
528 versus Nb (Fig. S2) show that the two Pascuales tonalites and the four LO dacites (~63–70
529 wt.% SiO_2) plot in the same compositional fields. The trondhjemitic samples extend these
530 fields toward high-silica rhyolitic compositions despite the gap between ~70 and ~78 wt.%
531 SiO_2. All these rocks share the same low concentrations in incompatible minor elements (Ti,
532 K, P) and extreme depletions in REE and Y (excepted one LO dacite enriched in K), that
533 distinguish them from the Rio Cala Arc dacites. Very low K_2O, TiO_2, HREE and Y
534 concentrations also characterize the Pujilí Granite, but the latter is characterized by much
535 higher La (40.2 ppm versus 3.7–5.0 ppm in Pascuales tonalites) and lower Yb (0.2 ppm
536 versus 0.7 ppm in Pascuales tonalites) concentrations, yielding strongly fractionated
537 normalized REE patterns (La/Yb_{CN} = 32 in Pujili Granite versus 3.6–4.7 in Pascuales
538 tonalites; Fig. 9A) indicative of residual garnet in the source of the Pujili Granite (Vallejo,
539 2007) but not in that of the Pascuales tonalites. As a whole, major element compositions of
540 Pascuales and LO felsic rocks form linear trends of decreasing MgO, Fe_2O_3, CaO, Al_2O_3,

P_2O_5 and Sr, and increasing Na_2O, La, Nb, Th and Zr with increasing SiO_2 (Figs 7 and 8). Excluding the two LO andesitic/dacitic samples more enriched in MgO, the Pascuales felsic rocks and the three LO MgO-poor dacites these trends appear to be consistent with fractional crystallization of plagioclase, amphibole ± pyroxene and apatite, as generally observed in the latest stages of differentiation of calc-alkaline magmatic series. From the tonalites to the trondhjemites, La/Yb_{CN} values slightly increase from 3.6–4.7 to 4.4–6.5. The latter also have lower concentrations in Y, HREE and MREE (Y and Sm vs. SiO_2 in Fig. 8), with concomitant decrease in $(Sm/Yb)_{PM}$ from 2.4 in the tonalites to 1.6 in the trondhjemites, whereas $(Zr/Sm)_{PM}$ increase from 1.3–1.5 in the tonalites to 2.2–3.8 in the trondhjemites. These features are interpreted as reflecting an increased control of the amphibole on the silica-richer liquid during magmatic differentiation (e.g., Davidson et al., 2007; Brophy, 2008; Dessimoz et al., 2012; Nandedkar et al., 2016; see section 8.2 for more details). The sample GD002 has the highest silica content and exhibits the strongest amphibole signature (Fig. 9B, C). This sample also displays a positive Eu anomaly, whereas the other two samples show no Eu anomalies. A positive Eu anomaly is generally thought to reflect plagioclase accumulation, but enrichment/depletion of Eu with respect to adjacent REE also result from competition between amphibole and plagioclase during fractionation (Tarney et al., 1979; Dessimoz et al., 2012) as suggested by higher Sr/Y ratios in the tonalites (Sr/Y = 31–32) with respect to the trondhjemites (Sr/Y = 9–16).

Cogenetic relationships are supported for the tonalites and trondhjemites which share similar $^{143}Nd/^{144}Nd$ ratios. However, the two LO MgO-rich samples (EQ94.1 and EQ94.2) analyzed by Reynaud et al. (1999) cannot have the same source composition as the Pascuales felsic rocks because they exhibit εNd_i values (+6.02 and +7.14, respectively) significantly higher than those of Pascuales tonalites and trondhjemites (+4.41 to +5.59). These two LO lavas contain Mg-rich pyroxene phenocrysts (Reynaud et al., 1999) and could be explained by

566 mixing between a felsic melt and a mafic (liquid or solid) component, as suggested by the
567 decrease of the εNd_i values with increasing SiO_2 and Nb contents (Fig. 11) and the linear
568 compositional trend in the MgO–SiO_2 binary diagram (Fig. 7). No isotopic data are available
569 for the other LO dacites and they are not directly associated on the field, therefore, they might
570 not be genetically related to Pascuales felsic rocks and might also plot on the same mixing
571 trends. Nevertheless, because both rock types share the same geochemical features and
572 display subparallel, similarly fractionated trace element patterns (Fig. 9), it is assumed that a
573 derivation from magmas having close compositions and/or that evolved via similar magmatic
574 processes took place.

575 Our new geochemical and chronological data together with previous regional
576 models allow to propose that: (i) the Pascuales tonalites can be considered as plutonic
577 equivalents of the LO dacites, representing a same magmatic episode; (ii) this magmatic
578 episode is middle-Coniacian, based on zircon dating of Pascuales intrusives, in agreement
579 with microfauna contained in LO sediments; (iii) the LO volcanites rest directly on the top of
580 the Piñón basalts, yielding a minimum late Turonian – early Coniacian age (~88–90 Ma) for
581 the basaltic exposure in this area (Luzieux et al., 2006; Ordoñez et al., 2006; van Melle et al.,
582 2008). LO volcanites and associated sediments are overlain by a thick pile of sediments of the
583 Calentura and Cayo Fms. dated, respectively, late-Coniacian to middle-Campanian, and
584 middle-late-Campanian (van Melle et al., 2008; Ordoñez et al., 2006). According to van Melle
585 et al. (2008) increasing abundance of volcanoclastic deposits and debris flows in the middle to
586 upper part of the Calentura Fm. suggests the onset of an instability period announcing the
587 construction of the San Lorenzo island arc. This arc was active from mid-Campanian to early-
588 middle Maastrichtian (~80–70 Ma) and was the source of the Cayo back-arc volcanoclastic
589 deposits. The short-lived Pascuales - LO magmatic episode exhibits atypical calc-alkaline
590 affinity and took place in the time interval (~90–80 Ma) that followed the final stage of

591 building of the oceanic plateau in coastal Ecuador and preceded self-substained subduction
592 zone beneath the San Lorenzo island arc. The possibility that this atypical magmatism was
593 related to initiation of the Late Cretaceous subduction at the leading edge of the CLIP will be
594 discussed section 8.3.2. Interestingly, the LO Member is intruded by dolerites (samples
595 04LD01 and 04GW-01 analyzed by Allibon et al., 2008) that display major, trace element and
596 lead and neodymium isotopic compositions within the range of the San Lorenzo and Rio Cala
597 tholeiitic basalts and basaltic andesites (Figs. 7 and 8); according to Luzieux (2007) these
598 intrusives would be coeval or younger than the Calentura Fm. and related to the San Lorenzo
599 arc.

600

601 *8.2 Geochemical constraints on the petrogenesis of Pascuales and Las Orquideas felsic rocks*

602

603 Small bodies of tonalites and trondhjemites (also referred as oceanic plagiogranites,
604 Coleman and Donato, 1979, see Koepke et al., 2007 for a review) and volcanic equivalents
605 are relatively common in thickened oceanic crust in all types of oceanic settings (mid-oceanic
606 ridges; back-arc spreading centers; plume-related plateau basalts; subduction zones) and in
607 ophiolites. Based on inferences from field relationships, trace element geochemistry and
608 isotope compositions, they are believed to represent products of either differentiated basaltic
609 magmas (e.g., Lippard et al., 1986; Amri et al., 1996; Floyd et al., 1998; Selbekk et al., 1998;
610 Rao et al., 2004; Bonev and Stampfli, 2009; Rollinson, 2009; Haase et al., 2016), or partial
611 melting of hydrated basalts, gabbros or sheeted dikes (e.g., Gerlach et al., 1981; Pedersen and
612 Malpas, 1984; Flagler and Spray, 1991; Floyd et al., 1998; Selbekk et al., 1998; Gillis and
613 Coogan, 2002; Koepke et al., 2007; Brophy, 2009; Rollinson, 2009; Brophy and Pu, 2012;

614 Tsuchiya et al., 2013; France et al., 2014), or both fractional crystallization and partial
615 melting of hydrated mafic rocks (Wanless et al., 2010).

616 Pascuales tonalites and LO dacites overlap in terms of most major elements with calc-
617 alkaline, silica-rich (63–75 wt.% SiO_2) experimental melts produced by crystal differentiation
618 of hydrated tholeiitic basaltic and andesitic magmas, as well as those produced by dehydration
619 melting of amphibolite and hydrous partial melting of basalt and gabbro, under varying
620 conditions of pressure, water content and oxygen fugacity (e.g., Dixon-Spulber and
621 Rutherford, 1983; Koepke et al., 2004; Berndt et al., 2005; Sisson et Kelemen, 2005; France
622 et al., 2010, 2014; Blatter et al., 2013; Nandedkar et al., 2014; Müntener and Ulmer, 2018,
623 among other; Fig. S3). Considering FeO*/MgO ratios and incompatible minor elements; the
624 Fig. 12 shows that Pascuales tonalites and LO dacites have the lowest FeO*/MgO ratios and
625 K_2O, TiO_2, P_2O_5 concentrations at given SiO_2 and MgO contents. Such low FeO*/MgO ratios
626 and extreme depletion in TiO_2 in dacitic compositions exclude an origin by fractional
627 crystallization of anhydrous tholeiites (e.g., Dixon-Spulber and Rutherford, 1983; Berndt et
628 al., 2005), and thus an origin of Pascuales tonalites and LO dacites by differentiation of Piñón
629 basaltic magmas. Instead they argue for a magmatic evolution under high water contents
630 and/or high oxidizing conditions. Low to very low K, Ti and P concentrations in experimental
631 dacites and rhyodacites and natural plutonic equivalents have been interpreted mainly as
632 reflecting depletions in the parent basalt (Dixon-Spulber and Rutherford, 1983; Beard and
633 Lofgren, 1991; Koepke et al., 2004; Berndt et al., 2005). Alternatively, water-saturated partial
634 melting of mafic rocks yields silicic melts with low FeO*/MgO and TiO_2 contents explained
635 by crystallization of Fe-Ti oxides (Beard and Lofgren, 1991), whereas low P_2O_5 contents may
636 reflect the presence of residual apatite in the solid residues (Wanless et al., 2010). For Koepke
637 et al. (2004, 2007), extreme depletion in TiO_2 contents in intermediate and silicic partial melts
638 reflects a refractory protolith and is a key parameter to discriminate between plagiogranite

639 generated by anatexis of hydrothermally altered cumulate gabbro from plagiogranite formed
640 by differentiation of basaltic magmas in the oceanic crust.

641 The anomalously low REE contents of the Pascuales tonalites and LO dacites with
642 respect to common calc-alkaline silicic rocks imply additional constraints. Amphibole is an
643 important hydrous phase that accommodates higher amounts of REE and other highly
644 incompatible elements than other major anhydrous phases (i.e., olivine, pyroxenes,
645 plagioclase) during the evolution of water-rich magmas. Because its stability increases with
646 increasing amount of water in the magma and with increasing pressure (Grove et al., 2003;
647 Barclay and Carmichael, 2004), its crystallization in water-rich, arc magmas in the lower crust
648 has for effects to dramatically reduce the REE increase rate and significantly modify
649 incompatible trace element ratios in the derivative melts (Davidson et al., 2007; Rodriguez et
650 al., 2007; Brophy, 2008; Rollinson, 2009; France et al., 2014; Nandedkar et al., 2016).
651 Similarly, amphibole, either as a residual phase (dehydration melting of amphibolite) or as a
652 reacting phase (hydrous partial melting), exerts a control over the REE in the low-degree,
653 silica-rich, partial melts from mafic rocks, because their incompatibility continuously
654 decreases with increasing liquid SiO_2 contents, eventually shifting from incompatible to
655 compatible (e.g., Sisson, 1994; Klein et al., 1997; Dalpe and Baker, 2000; Nandedkar et al.,
656 2016). Experimentally-based numerical models have explored the REE behaviors, absolute
657 abundances and degrees of enrichment (or enrichment factor F) in felsic magmas (~63–76
658 wt.% SiO_2) relative to the initial rock source or parent basalt for various compositions and
659 different depths and mechanisms of differentiation. They show that REE concentrations in
660 residual liquids slowly increase (F ~1.2–1.4, Brophy, 2008) or remain nearly constant (F ~0.5,
661 Rodriguez et al., 2007; F ~0.9, Nandedkar et al., 2016) over the entire range of differentiation
662 of arc magmas if amphibole is a major early fractionating phase at lower crustal pressures (≥
663 0.7 GPa, Alonzo-Perez et al., 2008; Blatter et al., 2013; Ulmer et al., 2018). Assuming that

Pascuales and LO dacitic magmas were generated after removal of ~50% of an amphibole-rich assemblage from a water-rich arc magma, such low enrichment factors would require less than ~2.8–4.2 ppm of La and less than ~0.4–0.6 ppm of Yb in the parent basaltic magmas, well below the REE contents of the more primitive Rio Cala basalts (Fig. 8) and other common arc basalts, suggesting derivation from water-rich, highly depleted magmas. In partial melting scenarios, enrichment factors calculated by Brophy (2008) vary between 2.1 and 3.2 for La and between 0.4 and 2.3 for Yb in derivative partial melts for a similar 63–70 wt.% SiO_2 range, regardless the type (equilibrium, fractional, accumulated fractional) and mechanism (dehydration oy hydration melting) of melting and compositions of the protolith. Application to Pascuales and LO dacitic rocks suggests strongly depleted rock sources containing 1.0–2.5 ppm of La and 0.3–1.8 ppm of Yb, more compatible with mafic–ultramafic cumulate protoliths rather than basaltic protoliths that solidified from slightly to moderately differentiated melts (see Fig. 12, France et al., 2014's experimental melting of MORB dykes).

Pascuales and LO felsics exhibit negative Nb anomalies in PM-normalized diagrams, a feature commonly attributed to an emplacement above a subduction zone. However, negative Nb anomalies is not always symptomatic of subduction settings as they are observed in Iceland and MOR dacites believed to be produced by low degrees of partial melting of hydrated oceanic crust (Gunnarsson et al., 1998; Haase et al., 2005; Wanless et al., 2010; Wilbold et al., 2009). Niobium is only moderately incompatible in amphibole equilibrated with silica-rich, calc-alkaline melts, with $D_{Nb/La}$ values above the unity, resulting in lower $(Nb/La)_{PM}$ in the felsic melts (Foley et al., 2002; Haase et al., 2005; Münker et al., 2004). In addition, Nb concentrations in melt are also controlled by magnetite and ilmenite as stable phases in the restite. The extremely low REE concentrations observed in Pascuales felsic rocks and LO dacites also explain the Zr and Hf positive anomalies on the PM-normalized

multi-element patterns, which are not observed in common tonalites and dacites. Like the REE, HFSE become more compatible in amphibole with increasing silica contents in melts (e.g., Foley et al., 2002; Nandedkar et al., 2016), but REE compatibility increases faster than HFSE compatibilities, while MREE are preferentially incorporated over LREE and HREE. As a result, Zr/Sm ratios increase with increasing silica contents in H_2O-rich liquids (Davidson, 2007; Nandedkar et al., 2016; Wanless et al., 2010).

In conclusion, major and trace element data (i.e., low FeO*/MgO, very low Ti and REE contents, high Zr/Sm ratios) suggest that the formation of Pascuales and LO felsic rocks result from magmatic processes largely dominated by amphibole and Fe-Ti oxides, implying evolution at high water contents. This conclusion is also consistent with the explosive emplacement of the LO dacites (van Melle et al., 2008). These conditions can be fulfilled by two magmatic processes, hydrous partial melting of mafic-ultramafic material or high-pressure, fractional crystallization of water-rich, arc-related magmas (or by a combination of both processes). Both models require fluxing of hydrous fluids in the crustal protoliths or in the mantle sources. However, amphibole alone cannot explain the REE extreme depletion; unusually depleted compositions of the protoliths or parent magmas are also needed.

8.3 Geodynamic implications

8.3.1 The partial melting of mafic cumulates evidence

Several aspects support a model invoking partial melting of mafic cumulates to generate Pascuales dacitic magma(s): 1) The Pascuales plutonic bodies are intrusive within basalts that unambiguously belong to the Piñón OPB, and both formations are almost contemporaneous, which implies that the OPB were still hot during the emplacement of the plutons. If, in addition, water was provided, the temperature needed for generating dacitic

713 melts from a gabbroic protolith (< 1000°C; e.g. Koepke et al., 2004, 2005) could have been
714 reached. 2) Natural examples in modern tectonic settings, experimental work and modelling
715 demonstrated that hydrous re-melting of mafic rocks yields K-poor calc-alkaline, rhyodacitic
716 magmas characterized by arc-like features such as negative Nb anomalies, independantly of
717 the origin of the protholith (N- and E-MORB-types or island-arc tholeiites) and of the tectonic
718 setting where partial melting took place (e.g. Haase et al., 2005; Wanless et al., 2010;
719 Willbold et al., 2009). In addition, other features such as the positive Zr anomalies and low
720 REE contents that distinguish the Pascuales felsics from common subduction-related dacites
721 are also characteristics of hydrous partial melts from mafic rocks.

722 The isotopic data exclude a common source for the Pascuales basalts and felsics.
723 However, a Piñón basalt sampled in the CCH (Ca1 in Fig. 10) exhibits a less radiogenic initial
724 $^{143}Nd/^{144}Nd$ composition (εNd_i = +4.49), slightly lower than those characterizing the tonalite
725 and trondhjemites, and plots below the fields of the CLIP and Galapagos Plume at 90 Ma
726 (Fig. 10A, B). Although this composition is unique among the six basalts analyzed in the
727 CCH (and among other Ecuadorian OPB), a few picrites and alkali basalts belonging to the
728 ~90–89 Ma oceanic plateau in Tortugal (Costa Rica; Hauff et al., 2000a; Trela et al., 2017)
729 and in the Beata Ridge (Caribbean Sea; Dürkefälden et al., 2019; Hauff et al., 2000a) have
730 εNd_i values (down to +4.24 and +5.41, respectively) lower than those of the basalts from the
731 Galapagos Plume. Indeed, the three Pascuales felsic rocks plot in a field defined by the
732 Tortugal magmatic rocks in the initial ($^{143}Nd/^{144}Nd$) versus ($^{206}Pb/^{204}Pb$) diagram (Fig. 10B),
733 suggesting that their protoliths could have derived from a mantle source region more enriched
734 than those of the main CLIP magmatic rocks. This mantle source region would be a mixture
735 of more radiogenic Nd and less radiogenic Pb isotopic compositions than common CLIP
736 rocks, and less radiogenic Nd and more radiogenic Pb isotopic compositions such as those
737 characterizing the Tortugal picrites and alkali basalts.

In the Ecuadorian Western Cordillera, early to late Cretaceous ultramafic and mafic rocks believed to represent lower crust fragments of the Pallantaga oceanic plateau such as the San Juan cumulates (Hughes and Pilatasig, 2002; Jaillard et al., 2009; Lapierre et al., 2000; Mamberti et al., 2004) and the Tortoras mafic granulites and amphibolites (Amortegui et al., 2011; Beaudon et al., 2005) (Fig. 2) also have the low REE and Ti compositions required to represent the protoliths of the Pascuales felsic magma. Nd-Sr-Pb isotopic data for these two terranes are shown in Fig. S4. The San Juan Unit exposes peridotites, layered werhlites, and layered and isotropic gabbros that yield a Sm/Nd isochron of 123 ± 13 Ma (Lapierre et al. 2000) and a zircon U/Pb age of 87.1 ± 1.6 Ma (Vallejo et al., 2006) and shows variable geochemical and isotopic compositions (Mamberti et al., 2004; Fig. S4A), indicating intercalation of two distinct magmatic sequences, possibly representing intrusions of a younger, Late Cretaceous, oceanic plateau magmas in an older, Early Cretaceous, oceanic plateau (Jaillard et al., 2009; Mamberti et al., 2004; Spikings et al., 2015; Vallejo et al., 2009). Values of εNd_i in San Juan cumulates range from +8.1 to +2.5 overlapping those of the Piñón OPB and Pascuales mafic and felsic rocks, but their ($^{206}Pb/^{204}Pb$) ratios are significantly lower (< 18.5; overlapping the picrites from the Guaranda terrane of the Pallatanga Unit; Mambeti et al., 2003), which precludes involvement of cumulates with similar isotopic compositions as protoliths of the Pascuales dacitic magma. The Tortoras granulite and amphibolites also span a wide range of $(^{143}Nd/^{144}Nd)_i$ (εNd_i values ranging from +7.9 to + 1.8) but display more radiogenic Sr and Pb isotopic compositions. The range of $(^{206}Pb/^{204}Pb)_i$ (18.72–19.07) is quite restricted and, in the initial ($^{143}Nd/^{144}Nd$) versus ($^{206}Pb/^{204}Pb$) diagram (Fig. S4B), their compositions overlap with those of Pascuales rocks. The amphibolites that have the lowest $(^{143}Nd/^{144}Nd)_i$ ratios are those that have the highest $(^{207}Pb/^{204}Pb)_i$ ratios (Fig. S4C) and $(^{208}Pb/^{204}Pb)_i$ (not shown), which is consistent with mixing with pelagic sediment. Such enrichments in radiogenic Pb likely occurred during the deformation and amphibolitisation of

763 the former basalts and cumulates. In contrast, isotopic compositions of the amphibolites the
764 least enriched in radiogenic Pb plot with the Pascuales felsic rocks in the Nd–Pb isotopic
765 spaces overlapping, or not far from, the OPB, Tortugal and Galapagos fields (Figs. S4 B, C),
766 indicating restricted or no contribution of sediment. Chemical and isotopic compositions of
767 Tortoras metamorphic cumulates thus compared well with the compositions expected for the
768 protoliths of Pascuales dacitic magma. However, low radiogenic Nd composition of the
769 trondhjemite CP603 is not correlated with higher values of $(^{207}Pb/^{204}Pb)_i$ and $(^{208}Pb/^{204}Pb)_i$
770 ratios, suggesting that its lower $(^{143}Nd/^{144}Nd)_i$ ratio may be a primary feature of the mantle
771 source region. The slight enrichments in radiogenic Pb observed in the samples GD001 and
772 GD003 with respect to CP603 indicate very small-scale variations likely reflecting post-
773 magmatic contamination.

774 High temperature metamorphism and granulite formation are commonly associated
775 with partial melting of the protolith. The metamorphism of the Tortoras rocks was dated
776 around 85 Ma in hornblende, a cooling age that post-dated the peak metamorphism (Vallejo et
777 al., 2006, 2009), which is also the age of the Pujili Granite (Vallejo et al., 2009). The granulite
778 and amphibolites experienced peak metamorphic conditions of 800°–850°C in the plagioclase
779 stability field (<6–9 kbar; Beaudon et al., 2005) and they include metamorphic mantle
780 peridotite in addition to metacumulate (Amortegui et al., 2011), therefore regional
781 metamorphism likely occurred at the crust – lithospheric mantle boundary, at the base of a
782 20–25 km thick oceanic crust consistent with the estimate thickness for the Caribbean plateau
783 crust (Mauffret and Leroy, 1997). It is reasonable to believe that similar lithologies
784 undergoing similar processes were also present at the base of the Piñón Fm. in the CCH,
785 providing possible sources for the Pascuales and LO felsic magmas (see also the deep crustal
786 xenolith suites in SW Colombia for similar lithologies, Weber et al., 2002). Further evidence
787 may be represented by the Piñón amphibole-bearing gabbros that yielded a cooling age of ca.

89 Ma (Luzieux et al., 2006) and which are now exposed ~20 km north of the Pascuales area. Indeed, the crystallization history of this gabbro may have coincided with melting of Piñón cumulates, and thus with the generation of the Pascuales and LO felsic magmas. Unfortunately, no detailed petrographic and geochemical data were published for these hornblende-bearing gabbros, so they may be interpreted as either a residual material of partial melting or as cumulates of arc magma differentiation, both types being almost petrographically indistinguishable (Ulmer et al., 2018).

In summary, major, trace and isotopic compositions are compatible with an origin of the Pascuales felsics by partial melting of mafic cumulates assumed to be present in the lower crust of the Piñón Fm. and possibly belonging to an older plume-related magmatic pulse or event. The protoliths might have derived from a mantle source region characterized by lower radiogenic Nd and more radiogenic Pb isotopic compositions than the common CLIP rocks. Alternatively, the low Nd radiogenic signature could result from addition of a small amount of pelagic sediments. It is assumed then that partial melting must have occurred in a hot and dynamic environment associated with deformation, hydration and metamorphism of mafic-ultramafic protholiths in deep-seated shear zones.

8.3.2 Felsic intrusions: a subduction initiation signature?

In several places in the Northwestern Andes and the Caribbean, the CLIP is intruded by gabbroic plutons and tonalitic batholiths with arc-like affinity signature; these plutons emplaced soon after the OPB extrusion and most of them are interpreted as crystallizion from juvenile, silicic magmas recording the initiation of an oceanic arc on the top of the oceanic plateau. These places include Western Colombia (e.g. Altamira, Zapata-Villada et al., 2017;

811 Buga, Villagomez et al., 2011; Bolivar Ultramafic Complex and Vijes (rhyodacitic) Felsites,
812 Kerr et al., 2004; Santa Fe and Burritica, Weber et al., 2015), Aruba (van de Lelij et al., 2010;
813 White et al, 1999; Wright and Wyld, 2011), Curaçao (Kerr et al., 1996 and Wright and Wyld,
814 2011); and Panama (Azuero Marginal Complex, Buchs et al, 2010). Some geochemical
815 similarities and differences between these felsic intrusions and the Pascuales and LO felsic
816 rocks are shown in Fig. S5. Compared to Pascuales tonalites, the Aruba, Santa Fe, Buritica
817 and Buga tonalites have higher overall REE abundances, but still lower than the Rio Cala
818 dacites, a difference that can be explained by refractory protholiths (gabbro cumulates) for
819 Pascuales and more enriched protoliths (basalts) for the other rocks. With the exception of the
820 Pujili Granite, all these rocks exhibit incompatible trace element contents and ratios indicating
821 that garnet had played no or very minor role as a residual phase, thus suggesting magma
822 generation at pressures lower than ~0.7 GPa. Like for LO volcanic rocks, these late
823 Cretaceous silicic intrusives have been interpreted as subduction-related based on calc-
824 alkaline affinities and Nb-Ta negative anomalies on N-MORB and PM-normalized multi-
825 element diagrams (see Whattam and Stern, 2015, for a review). However, as discussed in
826 Sections 8.2 and 8.3.1, partial melting of hydrated mafic rocks produces similar melt
827 compositions, and does not necessarily require plate subduction settings. In the other hand,
828 these intrusions occurred less than 10 Ma before steady-state, west-dipping subduction zones
829 beneath the San Lorenzo and Rio Cala intra-oceanic island arcs (see introductory section), a
830 time lag predicted by plate-tectonic models for the initiation of self-sustained subduction
831 zones (Stern and Gerya, 2018; Whattam and Stern, 2015). In this view, this silicic magmatism
832 that occurred shortly after (or even slightly overlap in time; van de Lelij et al., 2010; Whattam
833 and Stern, 2015) the eruption of the Piñón basalts can be interpreted as the earliest stage of
834 intra-oceanic subduction associated with widespread extension and asthenopheric upwelling

leading to the emplacement of basaltic magmas weakly or not affected by subduction fluids (Stern and Gerya, 2018).

On the basis of the lithologies and tectono-magmatic-metamorphic events recorded in Tortoras terrane, we propose that the hottest, deeper parts of the CCH oceanic plateau in Guayaquil area underwent similar high-temperature shear deformation and metamorphism and remelting triggered by intrusion and crystallization of younger mafic magmas in response to regional extension and asthenospheric upwelling. This agrees with crustal thickness estimates from forward modelling of potential data (Feininguer and Seguin, 1983; Aizprua et al., 2020) which define a ~7 km thick crust at the center-east CCH (i.e. 8 km thinner than unaffected plateau settings in west Ecuador). Without further evidence this thinning is tentatively ascribed to the same Late Cretaceous extensional episode. The composition of the upwelling mantle remains unknown since no basaltic lavas overly the top of the Piñón Fm. and the Ecuadorian OPB show no subduction contribution in their chemical signature (e.g. Hastie et al., 2013 and references therein). These underplating basalts could be either plume-related or hydrid between plume and arc as proposed by Whattam and Stern (2015) or arc basalts. A significant latent question is to know whether the Pascuales felsic rocks were co-magmatic or not with gabbroic and dioritic intrusions, as suggested by Pichler and Aly (1983) and Benitez (1995). Unfortunately, these rocks have not been clearly identified in the area and therefore, they have never been studied, nor dated. The lack of ~87–89 Ma aged mafic plutons intruded into the plateau and clearly identified as subduction-related and the lack of bimodal volcanism in the LO Member make not possible to firmly assert that the Pascuales and LO silicic magmatism was related to initiation of the San Lorenzo arc. We cannot exclude local remelting of the oceanic plateau without subduction (i.e., gravitational instability, subsidence effects); examples of juvenile, K-poor, calc-alkaline, dacitic magmas are reported in the Iceland basaltic plateau (Wilbold et al., 2009). However, sedimentary recordings in the

860 Calentura Fm. (van Melle et al., 2008), the wealth of petrologic and geochronologic data and
861 plate-tectonic models suggest that this region localized at the SW leading edge of the
862 Caribbean plateau was subjected to tectonic instability during or just after the end of plume-
863 related magmatism. Therefore, intrusions of new basaltic magmas during initiation of late
864 Cretaceous subduction are presently the best explanation for the partial melting of the mafic
865 rocks forming the Piñón Fm., as suggested for other tonalititc intrusions in the CLIP (e.g.,
866 Wright and Wyld, 2011; Weber et al., 2015).

867

868 **9. Conclusions**

869

870 1) Several 'granitic-like' igneous bodies intruded within basalts and metabasalts of the
871 Piñón Fm. (OPB part of the Caribbean Large Igneous Province, CLIP) in SW Ecuador near
872 the town of Pascuales. Petrographic and mineralogical analyses allow defining these
873 intrusions as tonalites and trondhjemites. Zircon U-Pb ages obtained by LA-ICP-MS yield ca.
874 ~87-89 Ma for one tonalite and two trondhjemites. Trace elements, field and chronological
875 data indicate that they are related to Las Orquideas dacitic breccias, which emplaced on the
876 Piñón Fm. during the Coniacian.

877 2) Geochemical compositions of the Pascuales felsic rocks are calc-alkaline but differ
878 from typical subduction-generated magmatic rocks by lower FeO*/MgO ratios, extreme
879 depletions in TiO_2 and P_2O_5, low La/Yb and moderately elevated Sr/Y ratios. In addition, on
880 primitive mantle-normalized multi-element diagrams, they are only moderately depleted in
881 Nb relative to La and enriched in Zr relative to Sm. Similar compositions are reproduced by
882 experiments and modeling of hydrous partial melting of mafic protoliths, and observed as
883 intrusions in oceanic crust in orogenic and anorogenic tectoning settings. However Pascuales

884 felsic rocks are characterized by extreme depletions in REE and Y, which are not observed in
885 other felsic intrusives of similar ages emplaced in the CLIP.

886 3) Isotope systematics (Nd-Sr-Pb) are robust for Nd and only marginally affected by
887 alteration for Sr and Pb data for the felsic bodies. Their isotope compositions overlap with the
888 field of the Caribbean oceanic plateau basalts, but plot at the least radiogenic Nd end-member
889 compositions.

890 4) The wealth of geochemical and isotopical data are consistent with partial melting of
891 hydrated OPB and can be accounted by a strong control of residual amphibole and Fe-Ti
892 oxides during the formation of the magmas. In addition, geochemical modeling and nature
893 analogues show that the extreme REE and Y concentrations require hydrous partial melting of
894 refractory mafic cumulates rather than less depleted basaltic protoliths.

895 5) The geochemical, chronological and geodynamic context suggest that both the
896 Pascuales and Las Orquideas felsic rocks represent silicic magmatism resulting from partial
897 melting of the deeper crust of the oceanic plateau during the final stage of its building. The
898 occurrence of this magmatism at the SW border of the CLIP, less than 10 Ma before the
899 activity of the subduction zones beneath the San Lorenzo - Rio Cala intra-oceanic island arcs,
900 suggests that the melting event may be related to the initiation of the subduction during Late
901 Cretaceous.

902

903 **Acknowledgements**

904 The manuscript greatly benefited from reviews by Etienne Jaillard and two anonymous
905 reviewers, they are all greatly acknowledged. We are indebted to Pablo Samaniego for the
906 Editorial process. This work was funded by the INSU (Institut National des Sciences de
907 l'Univers) du CNRS trough several scholarships attributed to CW.

References

Aizprua, C., Witt, C., Johansen, S.E., Barba, D., 2019. Cenozoic stages of forearc evolution following the accretion of a sliver from the Late Cretaceous-Caribbean Large Igneous Province: SW Ecuador-NW Peru. *Tectonics* 38, 1441–1465. https://doi.org/10.1029/2018TC005235

Aizprua, C., Witt, C., Bronner, M., Johansen, S.E., Barba, D., and Hernandez, M.J., 2020. Forearc crustal structure of Ecuador revealed by gravity and aeromagnetic anomalies and their geodynamic implications. *Lithosphere*. Article ID 2810692, 23. https://doi.org/10.2113/2020/2810692

Allibon, J., Monjoie, P., Lapierre, H., Jaillard, E., Bussy, F., Bosch, D., Senebier, F., 2008. The contribution of the young Cretaceous Caribbean Oceanic Plateau to the genesis of late Cretaceous arc magmatism in the Cordillera Occidental of Ecuador. *Journal of South American Earth Sciences* 26, 355–368. https://doi.org/10.1016/j.jsames.2008.06.003

Alonso-Perez, R., Müntener, O., Ulmer, P., 2008. Igneous garnet and amphibole fractionation in the roots of island arcs: experimental constraints on andesitic liquids. *Contributions to Mineralogy and Petrology* 157, 541–548. https://doi.org/10.1007/s00410-008-0351-8

Amórtegui, A., Jaillard, E., Lapierre, H., Martelat, J.-E., Bosch, D., Bussy, F., 2011. Petrography and geochemistry of accreted oceanic fragments below the Western Cordillera of Ecuador. *Geochemical Journal* 45, 57–78. doi:10.2343/geochemj.1.0091

Amri, I., Benoit, M., Ceuleneer, G., 1996. Tectonic setting for the genesis of oceanic plagiogranites: evidence from a paleo-spreading structure in the Oman ophiolite. *Earth Planetary Science Letters* 139, 177–194. https://doi.org/10.1016/0012-821X(95)00233-3

Anderson, J.L., Smith, D.R., 1995. The effects of temperature and fO_2 on the Al-in-hornblende barometer. *American Mineralogist* 80, 549–559. https://doi.org/10.2138/am-1995-5-614

Aspden, J.A., Litherland, M., 1992. The geology and Mesozoic collisional history of the Cordillera Real, Ecuador. *Tectonophysics* 205, 187–204. https://doi.org/10.1016/0040-1951(92)90426-7

Baker, J., Peate, D., Waight, T. & Meyzen C. , 2004. Pb isotopic analysis of standards and samples using a ^{207}Pb-^{204}Pb double spike and thallium to correct for mass bias with a double-focusing MC-ICPMS. *Chemical Geology* 211, 275-303.

Barclay, J., Carmichael, I.S.E., 2004. A hornblende basalt from Western Mexico: Water-saturated phase relations constrain a pressure–temperature window of eruptibility. *Journal of Petrology* 45, 485–506. https://doi.org/10.1093/petrology/egg091

Barker, F., 1979. Chapter 1 - Trondhjemite: Definition, Environment and Hypotheses of Origin. in: Barker, F., ed., Developments in Petrology, Trondhjemites, Dacites, and Related Rocks, Elsevier 6, 1–12. https://doi.org/10.1016/B978-0-444-41765-7.50006-X.

Beard, J.S., Lofgren, G.E., 1991. Dehydration Melting and Water-Saturated Melting of Basaltic and Andesitic Greenstones and Amphibolites at 1, 3, and 6. 9 kb. *Journal of Petrology* 32, 365–401. https://doi.org/10.1093/petrology/32.2.365

Beaudon, É., Martelat, J.-E., Amórtegui, A., Lapierre, H., Jaillard, E., 2005. Métabasites de la cordillère occidentale d'Équateur, témoins du soubassement océanique des Andes d'Équateur. *Comptes Rendus Géosciences* IIA 337, 625–634. https://doi.org/10.1016/j.crte.2005.01.002

Benitez, S., 1995. Evolution géodynamique de la province côtière sud-équatorienne au Crétacé supérieur-Tertiaire. *Géologie Alpine* 71, 3–163.

Berndt, J., Koepke, J., Holtz, F., 2005. An Experimental Investigation of the Influence of Water and Oxygen Fugacity on Differentiation of MORB at 200 MPa. *Journal of Petrology* 46, 135–167. https://doi.org/10.1093/petrology/egh066

Blatter, D.L., Sisson, T.W., Hankins, W.B., 2013. Crystallization of oxidized, moderately hydrous arc basalt at mid- to lower-crustal pressures: implications for andesite genesis. *Contributions to Mineralogy and Petrology* 166, 861–886. https://doi.org/10.1007/s00410-013-0920-3

Boland, M.L., Pilatasig, L.F., Ibadango, C.E., McCourt, W.J., Aspden, J.A., Hughes, R.A., Beate, B., 2000. Geology of the Cordillera Occidental of Ecuador between 0° and 1° N. Proyecto de Desarrollo Minero y Control Ambiental, programa de Informacion Cartografica y Geológica, British Geological Survey-CODIGEM, Dirección Nacional de Geología, Quito.

Bonev, N., Stampfli, G., 2008. Petrology, geochemistry and geodynamic implications of Jurassic island arc magmatism as revealed by mafic volcanic rocks in the Mesozoic low-grade sequence, eastern Rhodope, Bulgaria. Links Between Ophiolites and LIPs in Earth History. *Lithos* 100, 210–233. https://doi.org/10.1016/j.lithos.2007.06.019

Boschman, L. M., van Hinsbergen, D. J. J., Torsvik, T. H., Spakman, W., & Pindell, J. L. (2014). Kinematic reconstruction of the Caribbean region since the Early Jurassic. *Earth-Science Reviews* 138, 102–136. https://doi.org/10.1016/j.earscirev.2014.08.007

Brophy, J.G., 2009. La–SiO_2 and Yb–SiO_2 systematics in mid-ocean ridge magmas: implications for the origin of oceanic plagiogranite. *Contributions to Mineralogy and Petrology* 158, 99. https://doi.org/10.1007/s00410-008-0372-3

Brophy, J.G., 2008. A study of rare earth element (REE)–SiO_2 variations in felsic liquids generated by basalt fractionation and amphibolite melting: a potential test for discriminating between the two different processes. *Contributions to Mineralogy and Petrology* 156, 337–357. https://doi.org/10.1007/s00410-008-0289-x

Brophy, J.G., Pu, X., 2012. Rare earth element–SiO_2 systematics of mid-ocean ridge plagiogranites and host gabbros from the Fournier oceanic fragment, New Brunswick, Canada: a field evaluation of some model predictions. *Contributions to Mineralogy and Petrology* 164, 191–204. https://doi.org/10.1007/s00410-012-0732-x

Buchs, D.M., Arculus, R.J., Baumgartner, P.O., Baumgartner-Mora, C., Ulianov, A., 2010. Late Cretaceous arc development on the SW margin of the Caribbean Plate: Insights from the Golfito, Costa Rica, and Azuero, Panama, complexes. *Geochemistry Geophysics Geosystems* 11, 35 p. https://doi.org/10.1029/2009GC002901

Chiaradia, M., 2009. Adakite-like magmas from fractional crystallization and melting-assimilation of mafic lower crust (Eocene Macuchi arc, Western Cordillera, Ecuador). *Chemical Geology* 265, 468–487.

Chiaradia, M., Müntener, O., Beate, B., 2020, Effects of aseismic ridge subduction on the geochemistry of frontal arc magmas. *Earth Planetary Science Letters* 531, 115984. https://doi.org/10.1016/j.epsl.2019.115984.

Coleman, R.G., Donato, M.M., 1979. Chapter 5 - Oceanic Plagiogranite Revisited. in: Barker, F., ed., Developments in Petrology, Trondhjemites, Dacites, and Related Rocks. Develpments in petrology, Elsevier 6, 149–168. https://doi.org/10.1016/B978-0-444-41765-7.50010-1

Coogan, L.A., Wilson, R.N., Gillis, K.M., MacLeod, C.J., 2001. Near-solidus evolution of oceanic gabbros: insights from amphibole geochemistry. *Geochimica et Cosmochimica Acta* 65, 4339–4357. https://doi.org/10.1016/S0016-7037(01)00714-1

Cosma, L., Lapierre, H., Jaillard, E., Laubacher, G., Bosch, D., Desmet, A., Mamberti, M., Gabriele, P., 1998. Petrographie et geochimie des unites magmatiques de la Cordillere occidentale d'Equateur (0 degrees 30'); implications tectoniques. *Bulletin de la Société Géologique de France* 169, 739–751.

Dalpé, C., Baker, D.R., 2000. Experimental investigation of large-ion-lithophile-element-, high-field-strength-element- and rare-earth-element-partitioning between calcic amphibole and basaltic melt: the effects of pressure and oxygen fugacity. *Contributions to Mineralogy and Petrology* 140, 233–250. https://doi.org/10.1007/s004100000181

Davidson, J., Turner, S., Handley, H., Macpherson, C., Dosseto, A., 2007. Amphibole "sponge" in arc crust? *Geology* 35, 787–790. https://doi.org/10.1130/G23637A.1

Dessimoz, M., Müntener, O., Ulmer, P., 2012. A case for hornblende dominated fractionation of arc magmas: the Chelan Complex (Washington Cascades). *Contributions to Mineralogy and Petrology* 163, 567–589. https://doi.org/10.1007/s00410-011-0685-5

Dixon-Spulber, S., Rutherford, M.J., 1983. The Origin of Rhyolite and Plagiogranite in Oceanic Crust: An Experimental Study. *Journal of Petrology* 24, 1–25. https://doi.org/10.1093/petrology/24.1.1

Duncan, R.A., Hargraves, R.B., 1984. Caribbean region in the mantle reference frame. in: Bonini, W., Hargraves, R.B., Shagam, R., eds., The Caribbean-South American Plate Boundary and Regional Tectonics. *Geological Society of America Memoir*, 162, 89–121.

Dürkefälden, A., Hoernle, K., Hauff, F., Wartho, J-A., van den Bogaard, P., Werner, R., 2019. Age and geochemistry of the Beata Ridge: Primary formation during the main phase (~89 Ma) of the Caribbean Large Igneous Province. *Lithos* 328–329, 69–87. https://doi.org/10.1016/j.lithos.2018.12.021.

Egüez, A., Gaona, M., Albán, A., 2017. Mapa geológico de la República del Ecuador. Escala 1:1M. Inigemm.

Feininger, T., 1987. Allochthonous terranes in the Andes of Ecuador and northwestern Peru. *Canadian Journal of Earth Sciences* 24, 266–278.

Feininger, T., Seguin, M. K., 1983). Simple Bouguer gravity anomaly field and the inferred crustal structure of continental Ecuador. *Geology* 11(1), 40-44.

Flagler, P.A., Spray, J.G., 1991. Generation of plagiogranite by amphibolite anatexis in oceanic shear zones. *Geology* 19, 70–73. https://doi.org/10.1130/0091-7613(1991)019<0070:GOPBAA>2.3.CO;2

Floyd, P.A., Yaliniz, M.K., Goncuoglu, M.C., 1998. Geochemistry and petrogenesis of intrusive and extrusive ophiolitic plagiogranites, Central Anatolian Crystalline Complex, Turkey. *Lithos* 42, 225–241. https://doi.org/10.1016/S0024-4937(97)00044-3

Foley, S., Tiepolo, M., Vannucci, R., 2002. Growth of early continental crust controlled by melting of amphibolite in subduction zones. *Nature* 417, 837–840. https://doi.org/10.1038/nature00799

France, L., Koepke, J., Ildefonse, B., Cichy, S.B., Deschamps, F., 2010. Hydrous partial melting in the sheeted dike complex at fast spreading ridges: experimental and natural observations. *Contributions to Mineralogy and Petrology* 160, 683–704. https://doi.org/10.1007/s00410-010-0502-6

France, L., Koepke, J., MacLeod, C.J., Ildefonse, B., Godard, M., Deloule, E., 2014. Contamination of MORB by anatexis of magma chamber roof rocks: Constraints from a geochemical study of experimental melts and associated residues. *Lithos* 202–203, 120–137. https://doi.org/10.1016/j.lithos.2014.05.018

Gerlach, D.C., Leeman, W.P., Avé Lallemant, H.G., 1981. Petrology and geochemistry of plagiogranite in the Canyon Mountain ophiolite, Oregon. *Contributions to Mineralogy and Petrology* 77, 82–92. https://doi.org/10.1007/BF01161505

Gillis, K.M., Coogan, L.A., 2002. Anatectic Migmatites from the Roof of an Ocean Ridge Magma Chamber. *Journal of Petrology* 43, 2075–2095. https://doi.org/10.1093/petrology/43.11.2075

Gillis, K.M., Roberts, M.D., 1999. Cracking at the magma–hydrothermal transition: evidence from the Troodos Ophiolite, Cyprus. *Earth Planetary Science Letters* 169, 227–244. https://doi.org/10.1016/S0012-821X(99)00087-4

Gradstein, F.M., Ogg, J.G., Smith, A.G., 2004. A Geologic Time Scale 2004. *Cambridge University Press,* 589 pp.

Grove, T.L., Elkins-Tanton, L.T., Parman, S.W., Chatterjee, N., Müntener, O., Gaetani, G.A., 2003. Fractional crystallization and mantle-melting controls on calc-alkaline differentiation trends. *Contributions to Mineralogy and Petrology* 145, 515–533. https://doi.org/10.1007/s00410-003-0448-z

Gunnarsson, B., Marsh, B.D., Taylor, H.P., 1998. Generation of Icelandic rhyolites: silicic lavas from the Torfajökull central volcano. *Journal of Volcanology and Geothermal Research* 83, 1–45. https://doi.org/10.1016/S0377-0273(98)00017-1

Gutiérrez, G., Horton, B.K., Vallejo, C., Jackson, L.J., George, S.W.M., 2019. Chapter 9 - Provenance and geochronological insights into Late Cretaceous-Cenozoic foreland basin development in the Subandean Zone and Oriente Basin of Ecuador, 237–268. in: Andean Tectonics, Horton, B.K., Folguera, A. (eds.), Elsevier. https://doi.org/10.1016/B978-0-12-816009-1.00011-3.

Haase, K.M., Stroncik, N.A., Hékinian, R., Stoffers, P., 2005. Nb-depleted andesites from the Pacific-Antarctic Rise as analogs for early continental crust. *Geology* 33, 921–924. https://doi.org/10.1130/G21899.1

Hart, S.R., 1984. A large-scale isotope anomaly in the Southern Hemisphere mantle. *Nature* 309, 753–757. https://doi.org/10.1038/309753a0

Hastie, A.R., Mitchel, S.F., Treloar, P.J., Kerr, A.C., Neill, I., Barfod, D.N., 2013. Geochemical components in a Cretaceous island arc: The Th/La–$(Ce/Ce^*)_{Nd}$ diagram and implications for subduction initiation in the inter-American region. Lithos 162–163, 57–69. http://dx.doi.org/10.1016/j.lithos.2012.12.001.

Hauff, F., Hoernle, K., van der Bogard, P., 2000a. Age and geochemistry of basaltic complexes in western Costa Rica: contributions to the geotectonic evolution of Central America. *Geochemistry, Geophysics, Geosystems* 1, 1009. https://doi:10.1029/1999GC000020.

Hauff, F., Hoernle, K., Tilton, G., Graham, D.W., Kerr, A.C., 2000b. Large scale recycling of oceanic lithosphere over short time scales: geochemical constraints from the Caribbean Large Igneous Province. *Earth and Planetary Science Letters* 174, 247–263.

Helz, R.T., 1982. Phase relations and compositions of amphiboles produced in studies of the melting behavior of rocks. *Review in Mineralogy* 9B, 279–346.

Hofmann, A.W., 1988. Chemical differentiation of the Earth: the relationship between mantle, continental crust, and oceanic crust. *Earth Planetary Science Letters* 90, 297–314.

Hughes, R., Bermúdez, R. 1997. Geology of the Cordillera Occidental of Ecuador between 0°00´and 1° 00´S. Proyecto de desarollo minero y control ambiental, programa de información cartográfica y geológica. Report Number 4. British Geological Survey-CODIGEM, Quito, Ecuador, 75 pp.

Hughes, R.A., Pilatasig, L.F., 2002. Cretaceous and Tertiary terrane accretion in the Cordillera Occidental of the Andes of Ecuador. *Tectonophysics* 345, 29–48.

Jaillard, E., Lapierre, H., Ordonez, M., Alava, J.T., Amortegui, A., Vanmelle, J., 2009. Accreted oceanic terranes in Ecuador: southern edge of the Caribbean Plate? *Geological Society, London, Special Publication* 328, 469–485.

Jaillard, E., Ordonez, M., Suarez, J., Toro, J., Iza, D., Lugo, W., 2004. Stratigraphy of the late Cretaceous–Paleogene deposits of the Cordillera Occidental of central Ecuador: geodynamic implications. *Journal of South American Earth Sciences* 17, 49–58.

Kerr, Andrew C, Aspden, J.A., Tarney, J., Pilatasig, L.F., 2002a. The nature and provenance of accreted oceanic terranes in western Ecuador: geochemical and tectonic constraints. *Journal of the Geological Society, London* 159, 577–594.

Kerr, A.C., Marriner, G.F., Tarney, J., Nivia, A., Saunders, A.D., Thirlwall, M.F., Sinton, C.W., 1997. Cretaceous Basaltic Terranes in Western Columbia: Elemental, Chronological and Sr–Nd Isotopic Constraints on Petrogenesis. *Journal of Petrology* 38, 677–702. https://doi.org/10.1093/petroj/38.6.677

Kerr, A.C., Tarney, J., Kempton, P.D., Pringle, M., Nivia, A., 2004. Mafic Pegmatites Intruding Oceanic Plateau Gabbros and Ultramafic Cumulates from Bolívar, Colombia: Evidence for a 'Wet' Mantle Plume? *Journal of Petrology* 45, 1877–1906. https://doi.org/10.1093/petrology/egh037

Kerr, Andrew C., Tarney, J., Kempton, P.D., Spadea, P., Nivia, A., Marriner, G.F., Duncan, R.A., 2002b. Pervasive mantle plume head heterogeneity: Evidence from the late Cretaceous Caribbean-Colombian oceanic plateau. *Journal of Geophysical Research* 107, B7, 2140, 13 pp. https://doi.org/10.1029/2001JB000790

Kerr, A.C., Tarney, J., Marriner, G.F., Klaver, G.T., Saunders, A.D., Thirlwall, M.F., 1996. The geochemistry and petrogenesis of the late-Cretaceous picrites and basalts of Curaçao, Netherlands Antilles: a remnant of an oceanic plateau. *Contributions to Mineralogy and Petrology* 124, 29–43. https://doi.org/10.1007/s004100050171

Kerr, A.C., White, R.V., Thompson, P.M.E., Tarney, J., Saunders, A.D., 2003. No Oceanic Plateau—No Caribbean Plate? The Seminal Role of an Oceanic Plateau in Caribbean Plate Evolution, in C. Bartolini, R. T. Buffler, and J. Blickwede, eds., The Circum-Gulf of Mexico and the Caribbean: Hydrocarbon habitats, basin formation, and plate tectonics: *American Association of Petroleum Geologists Memoir* 79, 126–168.

Klein, M., Stosch, H.-G., Seck, H.A., 1997. Partitioning of high field-strength and rare-earth elements between amphibole and quartz-dioritic to tonalitic melts: an experimental study. *Chemical Geology* 138, 257–271. https://doi.org/10.1016/S0009-2541(97)00019-3

Koepke, J., Berndt, J., Feig, S.T., Holtz, F., 2007. The formation of SiO2-rich melts within the deep oceanic crust by hydrous partial melting of gabbros. *Contributions to Mineralogy and Petrology* 153, 67–84. https://doi.org/10.1007/s00410-006-0135-y

Koepke, J., Feig, S.T., Snow, J., 2005. Hydrous partial melting within the lower oceanic crust. *Terra Nova* 17, 286–291. https://doi.org/10.1111/j.1365-3121.2005.00613.x

Koepke, J., Feig, S.T., Snow, J., Freise, M., 2004. Petrogenesis of oceanic plagiogranites by partial melting of gabbros: an experimental study. *Contributions to Mineralogy and Petrology* 146, 414–432. https://doi.org/10.1007/s00410-003-0511-9

Lapierre, H., Bosch, D., Dupuis, V., Polvé, M., Maury, R.C., Hernandez, J., Monié, P., Yeghicheyan, D., Jaillard, E., Tardy, M., Lépinay, B.M. de, Mamberti, M., Desmet, A., Keller, F., Sénebier, F., 2000. Multiple plume events in the genesis of the peri-Caribbean Cretaceous oceanic plateau province. *Journal of Geophysical Research* 105, 8403–8421. https://doi.org/10.1029/1998JB900091

Leake, B.E., et al., 1978. Nomenclature of amphiboles: Report of the subcommittee on amphiboles of the International Mineralogical Association, commission on new minerals and mineral names. *The Canadian Mineralogist* 35, 219–246.

Lebrat, M., Mégard, F., Dupuy, C., Dostal, J., 1987. Geochemistry and tectonic setting of pre-collision Cretaceous and Paleogene volcanic rocks of Ecuador. *Geological Society American Bulletin* 99, 569-578.

Lippard, S.J., Shelton, A.W., Gass, I.G., 1986. The ophiolite of Northern Oman. *Geological Society, London, Memoir* 11, 178 pp.

Ludwig, K.R., 1998. On the Treatment of Concordant Uranium-Lead Ages. *Geochimica et Cosmochimica Acta* 62, 665–676. https://doi.org/10.1016/S0016-7037(98)00059-3

Ludwig, K. R. (2012). User's manual for Isoplot 3.75: A geochronological toolkit for Microsoft Excel, 75 pp. *Berkeley Geochronology Center, Special Publication,* (5).

Luzieux, L., 2007. Origin and late Cretaceous-Tertiary evolution of the Ecuadorian forearc. PhD thesis, ETH Zürich

Luzieux, L., Heller, F., Spikings, R., Vallejo, C., Winkler, W., 2006. Origin and Cretaceous tectonic history of the coastal Ecuadorian forearc between 1 N and 3 S: Paleomagnetic, radiometric and fossil evidence. *Earth Planetary Science Letters* 249, 400–414.

Macias, K.S., 2018. Geoquímica de los Plutones de Pascuales y de Bajo Grande (Cantón Jipijapa): dataciones U-Pb en zircones e implicaciones geodinámicas. PhD thesis, University of Guayaquil, Ecuador, 117pp.

Mamberti, M., Lapierre, H., Bosch, D., Jaillard, E., Ethien, R., Hernandez, J., Polvé, M., 2003. Accreted fragments of the Late Cretaceous Caribbean–Colombian Plateau in Ecuador. *Lithos* 66, 173–199. https://doi.org/10.1016/S0024-4937(02)00218-9

Mamberti, M., Lapierre, H., Bosch, D., Jaillard, E., Hernandez, J., Polvé, M., 2004. The Early Cretaceous San Juan Plutonic Suite, Ecuador: a magma chamber in an oceanic plateau? *Canadian Journal of Earth Science* 41, 1237–1258. https://doi.org/10.1139/e04-060

Manzotti, P., Poujol, M., Ballèvre, M., 2015. Detrital zircon geochronology in blueschist-facies meta-conglomerates from the Western Alps: implications for the late Carboniferous to early Permian palaeogeography. *Internal Journal of Earth Sciences* 104, 703–731.

Mauffret, A., Leroy, S., 1997. Seismic stratigraphy and structure of the Caribbean igneous province. *Tectonophysics* 283, 61–104.

McArthur, J.M., Howarth, R. J., and Bailey, T. R. , 2001. Strontium Isotope Stratigraphy: LOWESS Version 3: Best Fit to the Marine Sr-Isotope Curve for 0–509 Ma and Accompanying Look-up Table for Deriving Numerical Age. *Journal of Geology* 109, 155–170.

Miyashiro, A., 1974. Volcanic rock series in island arcs and active continental margins. *American Journal of Science* 274, 321–355. https://doi.org/10.2475/ajs.274.4.321

Morimoto, N., 1988. Nomenclature of Pyroxenes. *Mineralogy and Petrology* 39, 55–76. https://doi.org/10.1007/BF01226262

Münker, C., Wörner, G., Yogodzinski, G., Churikova, T., 2004. Behaviour of high field strength elements in subduction zones: constraints from Kamchatka–Aleutian arc lavas. *Earth Planetary Science Letters* 224, 275–293. https://doi.org/10.1016/j.epsl.2004.05.030

Müntener, O., Ulmer, P. (2018). Arc crust formation and differentiation constrained by experimental petrology. *American Journal of Science* 318, 64–89.

Nandedkar, R.H., Hürlimann, N., Ulmer, P., Müntener, O., 2016. Amphibole–melt trace element partitioning of fractionating calc-alkaline magmas in the lower crust: an experimental study. *Contributions to Mineralogy and Petrology* 171, 71. https://doi.org/10.1007/s00410-016-1278-0

Nandedkar, R.H., Ulmer, P., Müntener, O., 2014. Fractional crystallization of primitive, hydrous arc magmas: an experimental study at 0.7 GPa. *Contributions to Mineralogy and Petrology* 167, 1–27. https://doi.org/10.1007/s00410-014-1015-5

Ordoñez, M., Jiménez, N., and Suarez, J., 2006. Micropaleontología Ecuatoriana, datos bioestratigráficos y paleontológicos de las cuencas: Graben de Jambelí, Progreso, Manabí, Esmeraldas y Oriente; del levantamiento de la Península de Santa Elena, y de las cordilleras Chongón Colonche, costera y occidental. Petroproducción. Guayaquil: CIGG, 634 pp.

Pearce, J.A., 2014. Immobile Element Fingerprinting of Ophiolites. *Elements* 10, 101–108. https://doi.org/10.2113/gselements.10.2.101

Pedersen, R.B., Malpas, J., 1984. The origin of oceanic plagiogranites from the karmoy ophiolite, western Norway. *Contributions to Mineralogy and Petrology* 88, 36–52. https://doi.org/10.1007/BF00371410

Pichler, H., Aly, S., 1983. Neue K-Ar-Alter plutonischer Gesteine in Ecuador. *Zeitschrift der Deutschen Geologischen Gesellschaft* 134, 495–506.

Pin, C., Briot, D., Bassin, C., Poitrasson, F., 1994. Concomitant separation of strontium and samarium-neodymium for isotopic analysis in silicate samples, based on specific extraction chromatography. *Analytica Chimica Acta* 298(2), 209-217.

Plank, T., Langmuir, C.H., 1998. The chemical composition of subducting sediment and its consequences for the crust and mantle. *Chemical Geology* 145, 325–394.

Rao, D.R., Rai, H., Kumar, J.S., 2004. Origin of oceanic plagiogranite in the Nidar ophiolitic sequence of eastern Ladakh, India. *Current Science* 87, 999–1005.

Reynaud, C., Jaillard, É., Lapierre, H., Mamberti, M., Mascle, G.H., 1999. Oceanic plateau and island arcs of southwestern Ecuador: their place in the geodynamic evolution of northwestern South America. *Tectonophysics* 307, 235–254. https://doi.org/10.1016/S0040-1951(99)00099-2

Ridolfi, F., Renzulli, A., 2012. Calcic amphiboles in calc-alkaline and alkaline magmas: thermobarometric and chemometric empirical equations valid up to 1,130°C and 2.2 GPa. *Contributions to Mineralogy and Petrology* 163, 877–895. https://doi.org/10.1007/s00410-011-0704-6

Ridolfi, F., Renzulli, A., Puerini, M., 2010. Stability and chemical equilibrium of amphibole in calc-alkaline magmas: an overview, new thermobarometric formulations and application to subduction-related volcanoes. *Contributions to Mineralogy and Petrology* 160, 45–66. https://doi.org/10.1007/s00410-009-0465-7

Rodriguez, C., Sellés, D., Dungan, M., Langmuir, C., Leeman, W., 2007. Adakitic dacites formed by intracrustal ccrystal fractionation of water-rich parent magmas at Nevado de Longaví Volcano (36·2°S; Andean Southern Volcanic Zone, Central Chile). *Journal of Petrology* 48, 2033–2061. https://doi.org/10.1093/petrology/egm049

Rollinson, H., 2009. New models for the genesis of plagiogranites in the Oman ophiolite. The genesis and significance of adakitic, high-Mg andesites, and other refractory magmas in intra-oceanic forearc settings. *Lithos* 112, 603–614. https://doi.org/10.1016/j.lithos.2009.06.006

Selbekk, R.S., Furnes, H., Pedersen, R.-B., Skjerlie, K.P., 1998. Contrasting tonalite genesis in the Lyngen magmatic complex, north Norwegian Caledonides. *Lithos* 42, 243–268. https://doi.org/10.1016/S0024-4937(97)00045-5

Serrano, L., Ferrari, L., López, M., Petrone, C., and Jaramillo, C. 2011. An integrative geologic, geochronologic and geochemical study of Gorgona Island, Colombia: Implications for the formation of the Caribbean Large Igneous Province. *Earth and Planetary Science Letters* 309 (3-4), 324-336.

Sinton, C.W., Duncan, R.A., Storey, M., Lewis, J., Estrada, J.J., 1998. An oceanic flood basalt province within the Caribbean plate. *Earth Planetary Science Letters* 155, 221–235. https://doi.org/10.1016/S0012-821X(97)00214-8

Sisson, T.W., 1994. Hornblende-melt trace-element partitioning measured by ion microprobe. Trace-element Partitioning with Application to Magmatic Processes. *Chemical Geology* 117, 331–344. https://doi.org/10.1016/0009-2541(94)90135-X

Sisson, T. W., Ratajeski, K., Hankins, W. B., Glazner, A. F., 2005. Voluminous granitic magmas from common basaltic sources. *Contributions to Mineralogy and Petrology* 148, 635–661.

Sisson, T.W., Kelemen, P.B., 2018. Near-solidus melts of MORB + 4 wt% H_2O at 0.8–2.8 GPa applied to issues of subduction magmatism and continent formation. *Contributions to Mineralogy and Petrology* 173, 70. https://doi.org/10.1007/s00410-018-1494-x.

Spikings, R.A., Crowhurst, P., Winkler, W., Villagomez, D., 2010. Syn-and post-accretionary cooling history of the Ecuadorian Andes constrained by their in-situ and detrital thermochronometric record. *Journal of South American Earth Sciences* 30, 121–133.

Spikings, R.A., Cochrane, R., Villagomez, D., Van der Lelij, R., Vallejo, C., Winkler, W., Beate, B., 2015. The geological history of northwestern South America: from Pangaea to the early collision of the Caribbean Large Igneous Province (290–75 Ma). *Gondwana Research* 27, 195-139. https://doi.org/10.1016/j.gr.2014.06.004.

Stacey, J.S., Kramers, J.D., 1975. Approximation of terrestrial lead isotope evolution by a two-stage model. *Earth Planetary Science Letters* 26, 207–221. https://doi.org/10.1016/0012-821X(75)90088-6

Stern, R.J., and Gerya, T., 2018. Subduction initiation in nature and models: A review: *Tectonophysics* 746, 173–198. https://doi.org/10.1016/j.tecto.2017.10.014.

Sun, S.S., McDonough, W.F., 1989. Chemical and isotopic systematics of oceanic basalts: implications for mantle composition and processes. *Geological Society of America Special Paper* 42, 313–345. https://doi.org/10.1144/GSL.SP.1989.042.01.19

Tanaka, T., Togashi, S., Kamioka, H., Amakawa, H., Kagami, H., Hamamoto, T., et al., 2000. JNdi-1: a neodymium isotopic reference in consistency with LaJolla neodymium. *Chemical Geology* 168, 279-281.

Tarney, J., Weaver, B., Drury, S.A., 1979. Chapter 8 - Geochemistry of Archaean Trondhjemitic and Tonalitic Gneisses from Scotland and East Greenland, in: Barker, F., ed., Developments in Petrology, Trondhjemites, Dacites, and Related Rocks 6, 275–299, Elsevier. https://doi.org/10.1016/B978-0-444-41765-7.50013-7

Trela, J., Gazel, E., Sobolev, A. V., Moore, L., Bizimis, M., Jicha, B., Batanova, V.G., 2017. The hottest lavas of the Phanerozoic and the survival of deep Archaean reservoirs. *Nature Geoscience* 10 (6), 451–455.

Tsuchiya, N., Shibata, T., Yoshikawa, M., Adachi, Y., Miyashita, S., Adachi, T., Nakano, N., Osanai, Y., 2013. Petrology of Lasail plutonic complex, northern Oman ophiolite, Oman: An example of arc-like magmatism associated with ophiolite detachment. *Lithos* 156–159, 120–138. https://doi.org/10.1016/j.lithos.2012.10.013

Ulmer, P., Kägi, R., Müntener, O., 2018. Experimentally derived intermediate to silica-rich arc magmas by fractional and equilibrium crystallization at 1.0 GPa: An evaluation of phase relationships, compositions, liquid lines of descent and oxygen fugacity: *Journal of Petrology* 59, 11–58. https://doi.org/10.1093/ petrology/egy017.

Vallejo, C., Spikings, R.A., Luzieux, L., Winkler, W., Chew, D., Page, L., 2006. The early interaction between the Caribbean Plateau and the NW South American Plate. *Terra Nova* 18, 264–269.

Vallejo, C., Winkler, W., Spikings, R.A., Luzieux, L., Heller, F., Bussy, F., 2009. Mode and timing of terrane accretion in the forearc of the Andes in Ecuador. *Geological Society of America Special Paper* 204, 197–216.

Vallejo Cruz, C., 2007. Evolution of the Western Cordillera in the Andes of Ecuador (Late Cretaceous-Paleogene): [Ph.D. thesis]: Zürich, Switzerland, Institute of Geology, ETH Zürich, 208 pp. doi: 10.3929/ethz-a-010782581. https://doi.org/10.3929/ethz-a-005416411

Van der Lelij, R., Spikings, R.A., Kerr, A.C., Kounov, A., Cosca, M., Chew, D., Villagomez, D., 2010. Thermochronology and tectonics of the Leeward Antilles: evolution of the southern Caribbean Plate boundary zone. *Tectonics* 29, TC6003, 30 pp. doi:10.1029/ 2009tc002654.

Van Melle, J.V., Vilema, W., Faure-Brac, B., Ordoñez, M., Lapierre, H., Jimenez, N., Jaillard, E., Garcia, M., 2008. Pre-collision evolution of the Piñón oceanic terrane of SW

Ecuador: stratigraphy and geochemistry of the Calentura Formation. *Bulletin de la Société Géologique de France* 179, 433–443. https://doi.org/10.2113/gssgfbull.179.5.433

Van Thournout, F. 1991. Stratigraphy, magmatism and tectonism in the Ecuadorian northwestern cordillera: Metallogenic and Geodynamic implications. PhD thesis, Katholieke Universiteit Leuven, 150 pp.

Velasco, S. M-L. Mendoza, I.K., 2003. Estudio geológico del Miembro Calentura de la Formación Cayo en el flanco oriental de la Cordillera Chongón-Colonche. – Thesis Ing. Universidad de Guayaquil, 182 pp.

Villagómez, D., Spikings, R., Magna, T., Kammer, A., Winkler, W., Beltrán, A., 2011. Geochronology, geochemistry and tectonic evolution of the Western and Central cordilleras of Colombia. *Lithos* 125, 875–896. https://doi.org/10.1016/j.lithos.2011.05.003

Wanless, V.D., Perfit, M.R., Ridley, W.I., Klein, E., 2010. Dacite petrogenesis on mid-ocean ridges: Evidence for oceanic crustal melting and assimilation. *Journal of Petrology* 51, 2377–2410.

Weber, M.B.I., Gómez-Tapias, J., Cardona, A., Duarte, E., Pardo-Trujillo, A., Valencia, V.A., 2015. Geochemistry of the Santa Fé Batholith and Buriticá Tonalite in NW Colombia – Evidence of subduction initiation beneath the Colombian Caribbean Plateau. *Journal of South American Earth Sciences* 62, 257–274. https://doi.org/10.1016/j.jsames.2015.04.002

Weber, M.B.I., Tarney, J., Kempton, P.D., Kent, R.W., 2002. Crustal make-up of the northern Andes: evidence based on deep crustal xenolith suites, Mercaderes, SW Colombia. *Tectonophysics* 345, 49–82.

Whattam, S.A., Stern, R.J., 2015. Late Cretaceous plume-induced subduction initiation along the southern margin of the Caribbean and NW South America: The first documented example with implications for the onset of plate tectonics. *Gondwana Research* 27, 38–63. https://doi.org/10.1016/j.gr.2014.07.011

White, R.V., Tarney, J., Kerr, A.C., Saunders, A.D., Kempton, P.D., Pringle, M.S., Klaver, G.T., 1999. Modification of an oceanic plateau, Aruba, Dutch Caribbean: Implications for the generation of continental crust. *Lithos* 46, 43–68. https://doi.org/10.1016/S0024-4937(98)00061-9

Wilkinson, I.P., 1998. Foraminifera from a suite of Late Cretaceous to Palaeogene samples of the Cordillera occidental, Ecuador. Technical Report WH/98/163R Biostratigraphy and Sedimentology Group, British Geological Survey. Nottingham UK.

Willbold, M., Hegner, E., Stracke, A., Rocholl, A., 2009. Continental geochemical signatures in dacites from Iceland and implications for models of early Archaean crust formation. *Earth Planetary Science Letters* 279, 44–52. doi:10.1016/j.epsl.2008.12.029

Witt, C., Reynaud, J.Y., Barba, D., Poujol, M., Aizprua, C., Rivadeneira, M., Amberg, C., 2019. From accretion to forearc basin initiation: The case of SW Ecuador, Northern Andes. *Sedimentary Geology* 379, 138–157. https://doi.org/10.1016/j.sedgeo.2018.11.009

Witt, C., Rivadeneira, M., Poujol, M., Barba, D., Beida, D., Beseme, G., Montenegro, G., 2017. Tracking ancient magmatism and Cenozoic topographic growth within the Northern Andes forearc: Constraints from detrital U-Pb zircon ages. *Geological Society of America Bulletin* 129, 415–428. https://doi.org/10.1130/B31530.1

Wright, J.E., Wyld, S.J., 2011. Late Cretaceous subduction initiation on the eastern margin of the Caribbean-Colombian Oceanic Plateau: One Great Arc of the Caribbean (?). *Geosphere* 7, 468–493. https://doi.org/10.1130/GES00577.1

Zapata-Villada, J.P., Restrepo, J.J., Cardona-Molina, A., Martens, U., 2017. Geoquímica y geocronología de las rocas volcánicas básicas y el Gabro de Altamira, Cordillera Occidental (Colombia): Registro de ambientes de Plateau y arco oceánico superpuestos durante el cretácico. *Boletín de Geología* 39 (2), 13–30.

Zindler, A., Hart, S., 1986. Chemical geodynamics. Annu. Rev. *Earth Planetary Science Letters* 14, 493–571.

Figure Captions

Fig. 1. (A) Plume-induced subduction initiation model of the Caribbean Large Igneous Province (CLIP) between 89-85 Ma (modified from Whattam and Stern, 2014). Green areas show supposed active arcs. (B) Geodynamic cartoon showing the configuration of central-south Ecuador and north Peru. Abbreviations are as follows: AM, Amotapes massif; CCH, Chongón-Colonche hills; JF, Jubones fault; NAP, North American plate; SAP, South American plate; WC, Western Cordillera.

Fig. 2. (A) Geological map of the Western Cordillera and forearc areas of Ecuador (Eguez et al., 2017). (B) Simplified geologic columns representative of western Ecuador. Abbreviations are as follows: CCH, Chongón-Colonche Hills; MB, Manabí basin; PB, Progreso basin; PG, Pujilí Granite; TA, Tortoras amphibolite; SJ, San Juan Unit; POPB, Pinon oceanic plateau basal; WC, Western Cordillera.

Fig. 3. (A) Aerial view of the Pascuales area (Google Earth image) showing sample location and the intrusive bodies (red polygons). (B, C) Field photogaphies of tonalitic and trondhjemitic outcrops. (D) Field photography of the basalt GD004. The asterisk refers to dated samples.

Fig. 4. Composition of clinopyroxenes and amphiboles from the studied Pascuales rocks. (A) Pyroxenes from the metabasalts CP605 and GD004 in the Mg-Ca-Fe diagram of Morimoto et al. (1998). (B) Variation of Al_2O_3 (wt. %) vs. Mg# in CP605 and GD004 clinopyroxenes. (C) Variation of Mg# vs. Si in amphiboles from the tonalite CP601 and the metabasalts CP605 and CP607. (D) Variations of $(Na + K)_A$ vs. Al^{IV} in amphiboles from the tonalite CP601 and the metabasalts CP605 and CP607. In panels (C) and (D), relicts of aluminous amphiboles preserved in late-stage magnesio-hornblendes are circled. Numbers of atomes par formula unit (apfu) in amphiboles are calculated on the basis of 13 cations excluding Ca, Na, K. Nomenclature of amphiboles from Leake et al. (1997). Sample locations are shown on Fig. 3.

Fig. 5. (A) Terra Wasserburg diagram for the tonalite CP024. (B) Terra Wasserburg diagram for the tonalite CP601. (C) Terra Wasserburg diagram for the trondhjemite CP603.

1521

1522 Fig. 6. Normative Ab-An-Or plots of the Pascuales felsic plutonic rocks (this study) along
1523 with Las Orquideas volcanic rocks (data from Reynaud et al., 1999 and van Melle et al.,
1524 2008). Fields are after Baker (1979): tonalites (To), trondhjemites (Tr), granodiorites (Gd)
1525 and granites (Gr).

1526

1527 Fig.7. Harker diagrams showing major oxide variations against SiO_2 (wt.%) of the studied
1528 Pascuales basaltic lavas and felsic plutonic rocks. Other late Cretaceous Ecuadorian magmatic
1529 rocks are projected for comparison with the studied rocks; data are from: (1) Reynaud et al.
1530 (1999), Kerr et al. (2002a), Mamberti et al. (2003), Vallejo (2007), Chiarada (2009), and
1531 Allibon et al. (2008) for Ecuadorian oceanic plateau basalts (OPB); Piñón basalts collected in
1532 the Chongón-Colonche Hills (CCH) have been distinguished by a black spot. (2) Reynaud et
1533 al. (1999) and van Melle et al. (2008) for Las Orquideas (LO) volcanic rocks, and from
1534 Allibon et al. (2008) for the dolerites. (3) Cosma et al. (1998), Reynaud et al. (1999), Kerr et
1535 al. (2002a), Vallejo (2007), Allibon et al. (2008), and Chiarada (2009), for island arc volcanic
1536 rocks of the San Lorenzo Fm. and Rio Cala Arc. (4) Vallejo (2007) for the Pujili Granite.

1537

1538 Fig. 8. Variations of selected incompatible trace element contents (ppm) against SiO_2 (wt.%)
1539 for the studied Pascuales basaltic lavas and felsic plutonic rocks. Data sources for other Late
1540 Cretaceous Ecuador magmatic rocks same as Fig. 7.

1541

Fig. 9. (A) Chondrite-normalized REE patterns of Pascuales tonalitic samples. (B) Chondrite-normalized REE patterns of Pascuales trondhjemitic samples. (C) Multi-element patterns normalized to primitive mantle (PM) of Pascuales tonalitic and trondhjemitic samples. (D) Chondrite-normalized REE patterns of Pascuales basaltic samples. (E) Multi-element patterns normalized to N-MORB of Pascuales basaltic samples. In panels A–C gray field is for Rio Cala Arc volcanic rocks with $SiO_2 \geq 56$ wt.%. In panel D gray field is for other Ecuador oceanic plateau basalts and dolerites. Data sources for Las Orquideas, Rio Cala Arc and oceanic plateau magmatic rocks same as Fig. 7. Normalizing values are from Sun and McDonough (1989).

Fig. 10. Initial Nd, Sr and Pb isotope plots of the studied Pascuales basaltic lavas and felsic plutonic rocks. Data for Ecuadorian OPB and Piñón (CCH) basalts and dolerites are from Reynaud et al. (1999), Mamberti et al. (2003), Vallejo (2007) and Lapierre et al. (2000). Data for Rio Cala Arc and San Lorenzo Fm. volcanic rocks are from Cosma et al. (1998), Reynaud et al. (1999), Vallejo (2007), Allibon et al. (2008) and Chiarada (2009). In (A) the two Las Orquideas (LO) samples are the MgO-rich, silica-rich volcanic rocks (Reynaud et al., 1999); no isotope data have been published for the LO Mg-poor dacitic samples; in (B–D) data for LO dolerites are from Allibon et al. (2008). Are also reported Tortugal picrites and alkali basalts from Hauff et al. (2000a) and Trela et al. (2017). The fields of the Galapagos Plume, Pacific N-MORB and pelagic sediments at 90 Ma are from Hauff et al. (2000a,b) and the field of the Caribbean Large Igneous Province (CLIP) is after Kerr et al. (1996, 1997). The global composition of subducting sediment (GLOSS) is Plank and Langmuir (1998), the Northern Hemisphere Reference Line (NHRL) is from Hart (1984) and the Bulk Silicate Earth (BSE) is from Zindler and Hart (1986).

Fig. 11. Variations of initial radiogenic Nd isotope vs. SiO_2 (wt. %) and Nb (ppm) for the Pascuales basaltic lavas and felsic plutonic rocks and the two Las Orquideas (LO) MgO-rich, silicica-rich volcanic rocks rocks (data from Reynaud et al., 1999). No isotopic data are available for the LO MgO-poor dacites.

Fig. 12. Comparison of Pascuales felsic (this study) and Las Orquideas (LO) dacitic compositions with melt compositions from experiments in Harker-type diagrams. (A) K_2O vs. SiO_2. (B) P_2O_5 vs. SiO_2. (C) FeO*/MgO vs. SiO_2. (D) TiO_2 vs. MgO. Experimental data for fractional crystallization (FC) of arc magmas at mid to lower crustal depths: Sisson et al. (2005), Blatter et al. (2013), Nandedkar et al. (2014), and Ulmer et al. (2018). Experimental data for hydrous partial melting (HPM) of rocks: Koepke et al. (2004) for hydrous partial melting of oceanic cumulate gabbros and France et al. (2010, 2014) for anatexis of hydrothermally altered mid-oceanic ridge sheeted dikes. Initial (in.) compositions of the gabbro protoliths (Koepke et al., 2004) are also shown. Tholeiitic (TH) and calc-alkaline (CA) fields are from Miyashiro (1974). High FeO*/MgO ratios of Pascuales trondhjemites are due to very low MgO contents.

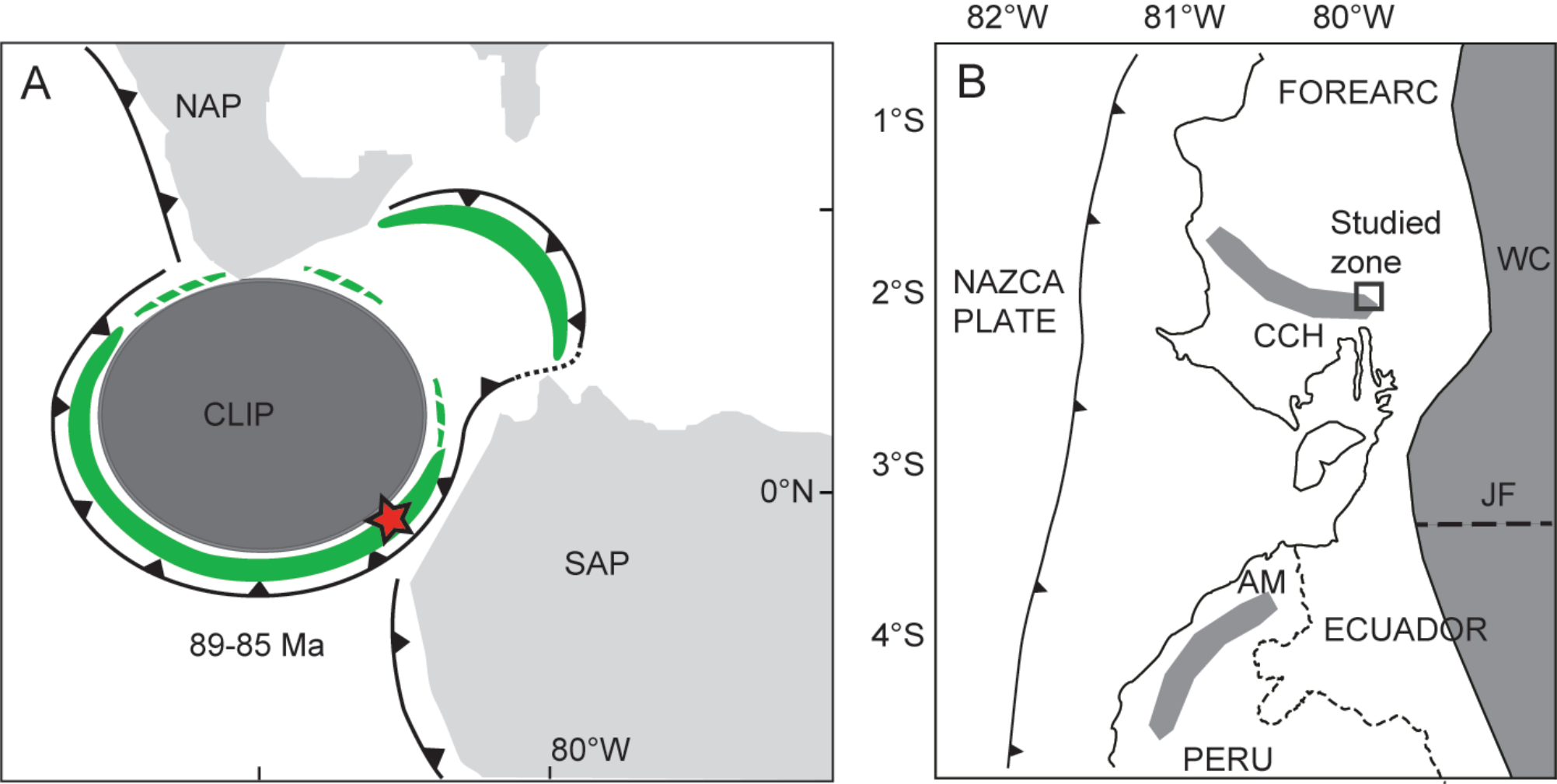
A
NAP
CLIP
SAP
89-85 Ma
0°N
80°W
B
82°W
81°W
80°W
1°S
2°S
3°S
4°S
FOREARC
Studied
zone
WC
NAZCA
PLATE
CCH
JF
AM
ECUADOR
PERU

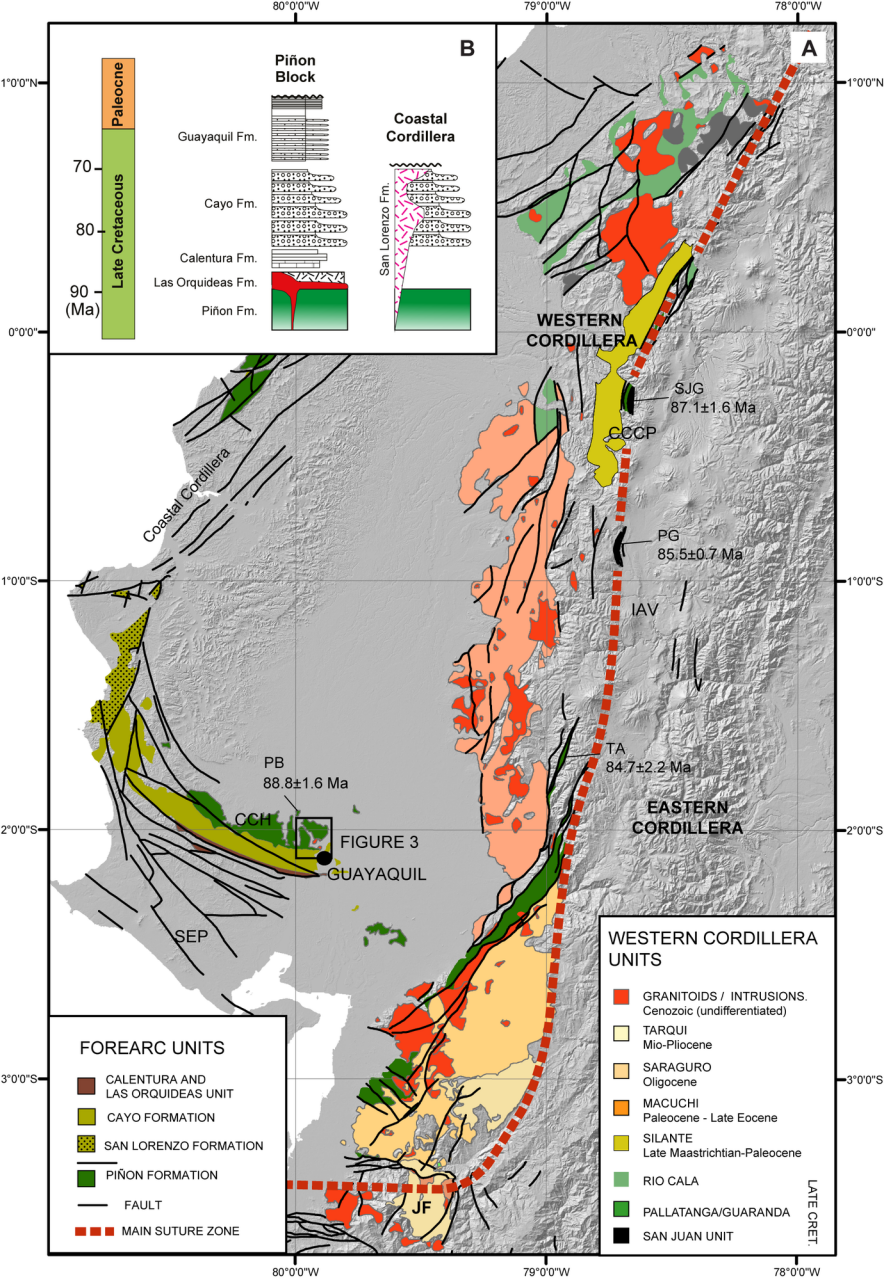
80°0'0"W
79°0'0"W
78°0'0"W
1°0'0"N
0°0'0"
1°0'0"S
2°0'0"S
3°0'0"S
A
B
Paleocene
Late Cretaceous
70
80
90
(Ma)
Piñon Block
Guayaquil Fm.
Cayo Fm.
Calentura Fm.
Las Orquideas Fm.
Piñon Fm.
Coastal Cordillera
San Lorenzo Fm.
WESTERN CORDILLERA
SJG
87.1±1.6 Ma
CCCP
PG
85.5±0.7 Ma
IAV
TA
84.7±2.2 Ma
EASTERN CORDILLERA
Coastal Cordillera
PB
88.8±1.6 Ma
CCH
FIGURE 3
GUAYAQUIL
SEP
JF
FOREARC UNITS
CALENTURA AND LAS ORQUIDEAS UNIT
CAYO FORMATION
SAN LORENZO FORMATION
PIÑON FORMATION
FAULT
MAIN SUTURE ZONE
WESTERN CORDILLERA UNITS
GRANITOIDS / INTRUSIONS. Cenozoic (undifferentiated)
TARQUI Mio-Pliocene
SARAGURO Oligocene
MACUCHI Paleocene - Late Eocene
SILANTE Late Maastrichtian-Paleocene
RIO CALA
PALLATANGA/GUARANDA
SAN JUAN UNIT
LATE CRET.

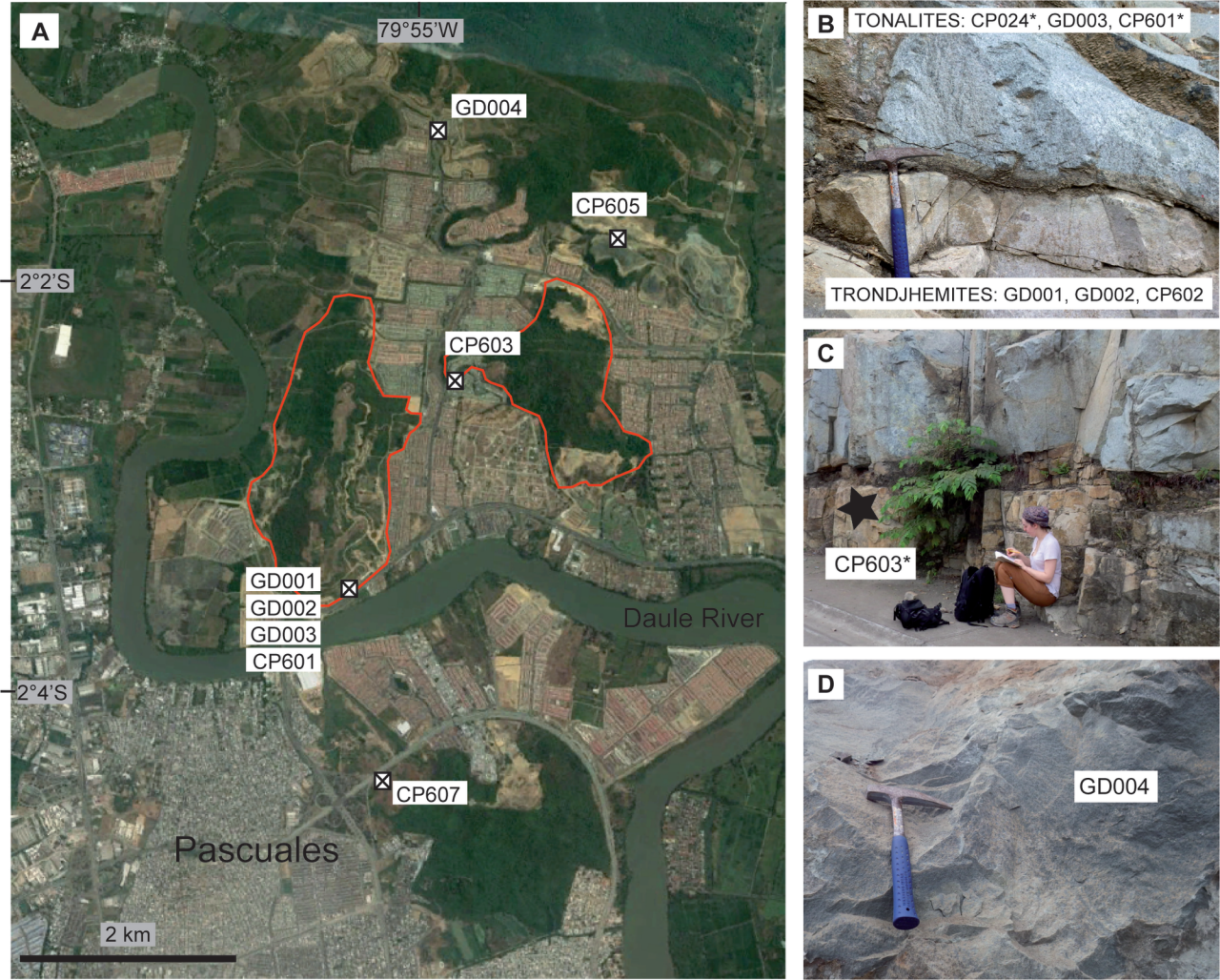
A
79°55'W
GD004
CP605
2°2'S
CP603
GD001
GD002
GD003
CP601
Daule River
2°4'S
CP607
Pascuales
2 km
B
TONALITES: CP024*, GD003, CP601*
TRONDJHEMITES: GD001, GD002, CP602
C
CP603*
D
GD004

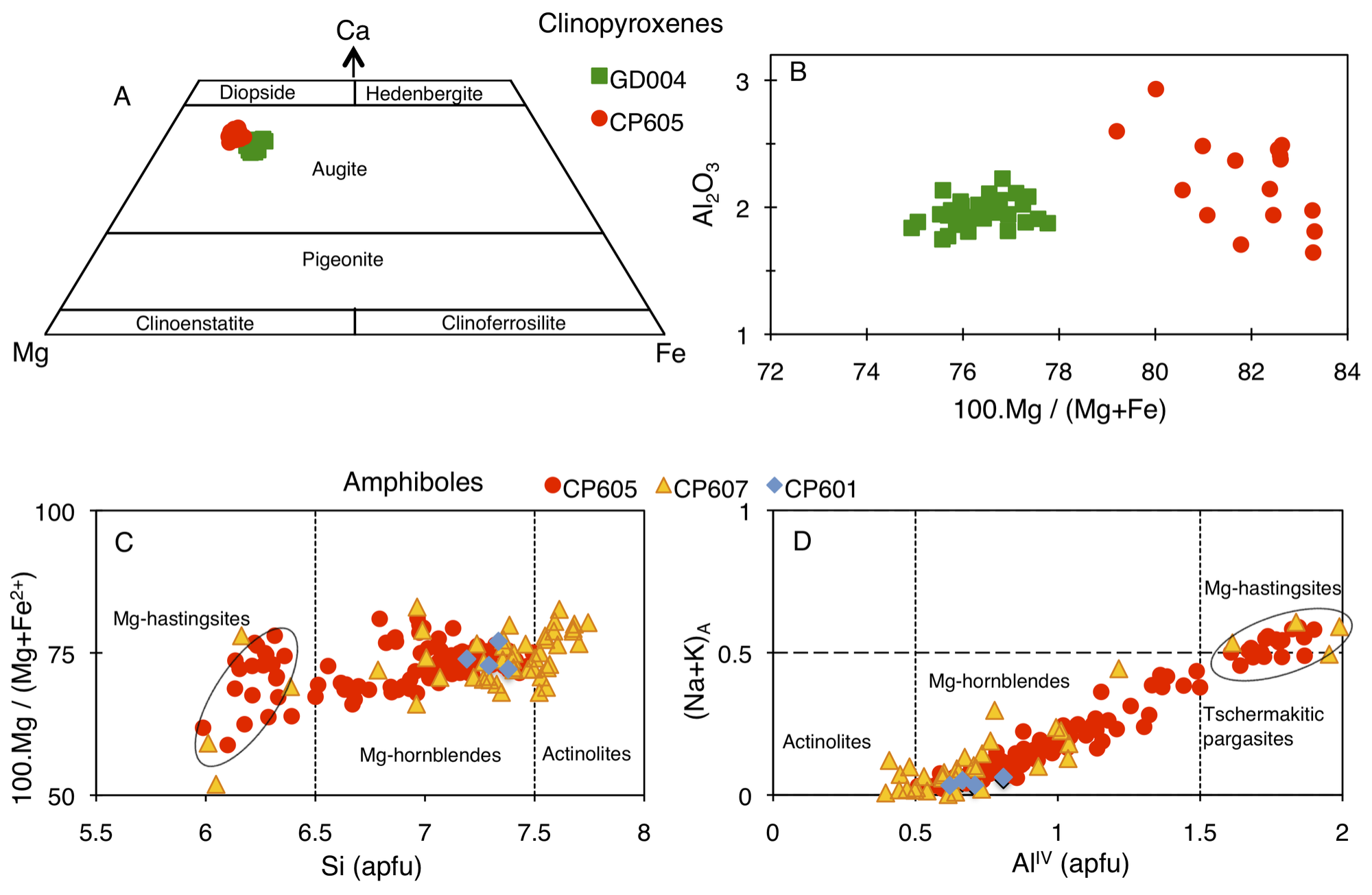
Clinopyroxenes
Ca
A
Diopside
Hedenbergite
Augite
Pigeonite
Clinoenstatite
Clinoferrosilite
Mg
Fe
GD004
CP605
B
Al_2O_3
100.Mg / (Mg+Fe)
Amphiboles
CP605
CP607
CP601
C
Mg-hastingsites
Mg-hornblendes
Actinolites
100.Mg / (Mg+Fe^{2+})
Si (apfu)
D
Mg-hastingsites
Mg-hornblendes
Tschermakitic pargasites
Actinolites
$(Na+K)_A$
Al^{IV} (apfu)

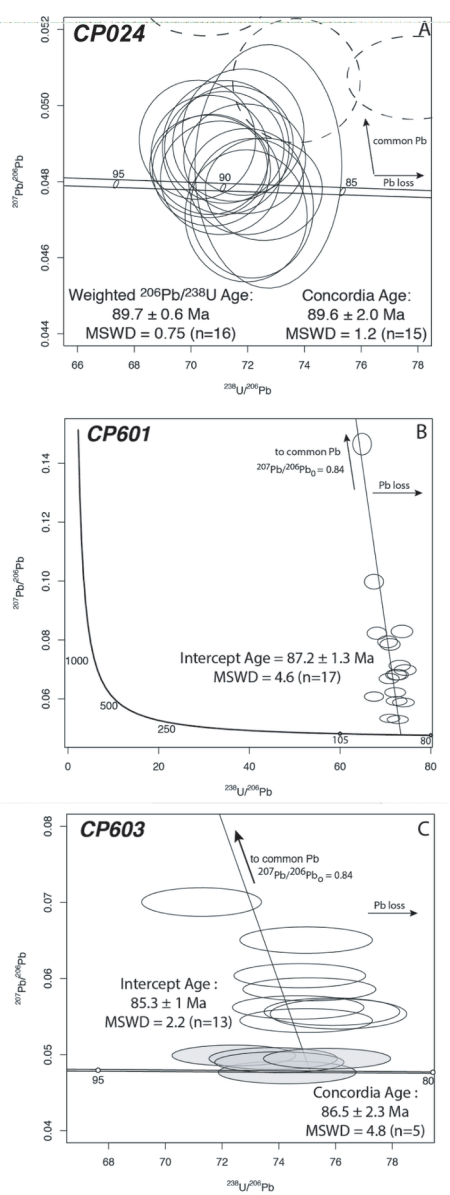

Figure 5. Seyler et al.

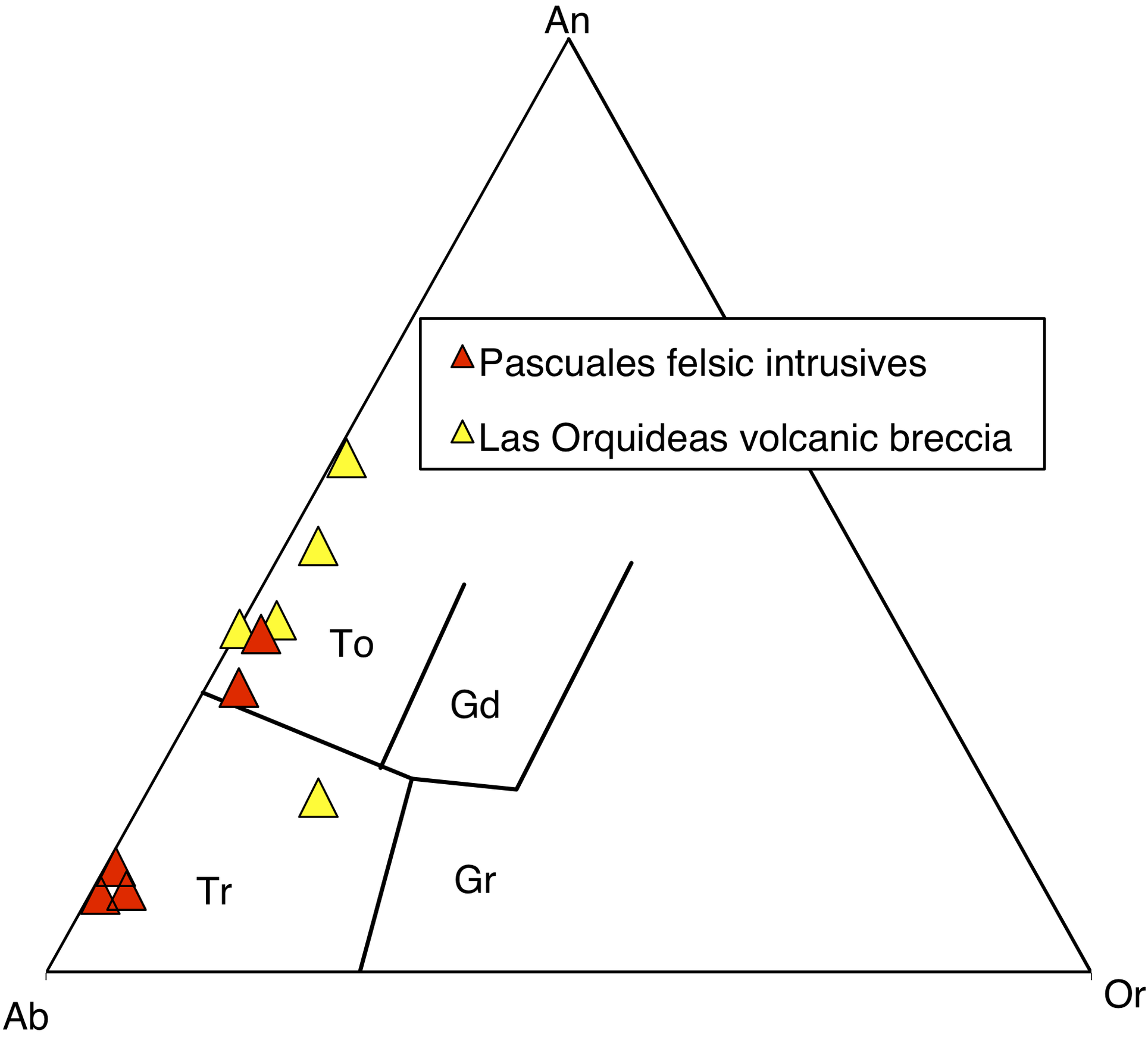
An
Pascuales felsic intrusives
Las Orquideas volcanic breccia
To
Gd
Tr
Gr
Ab
Or

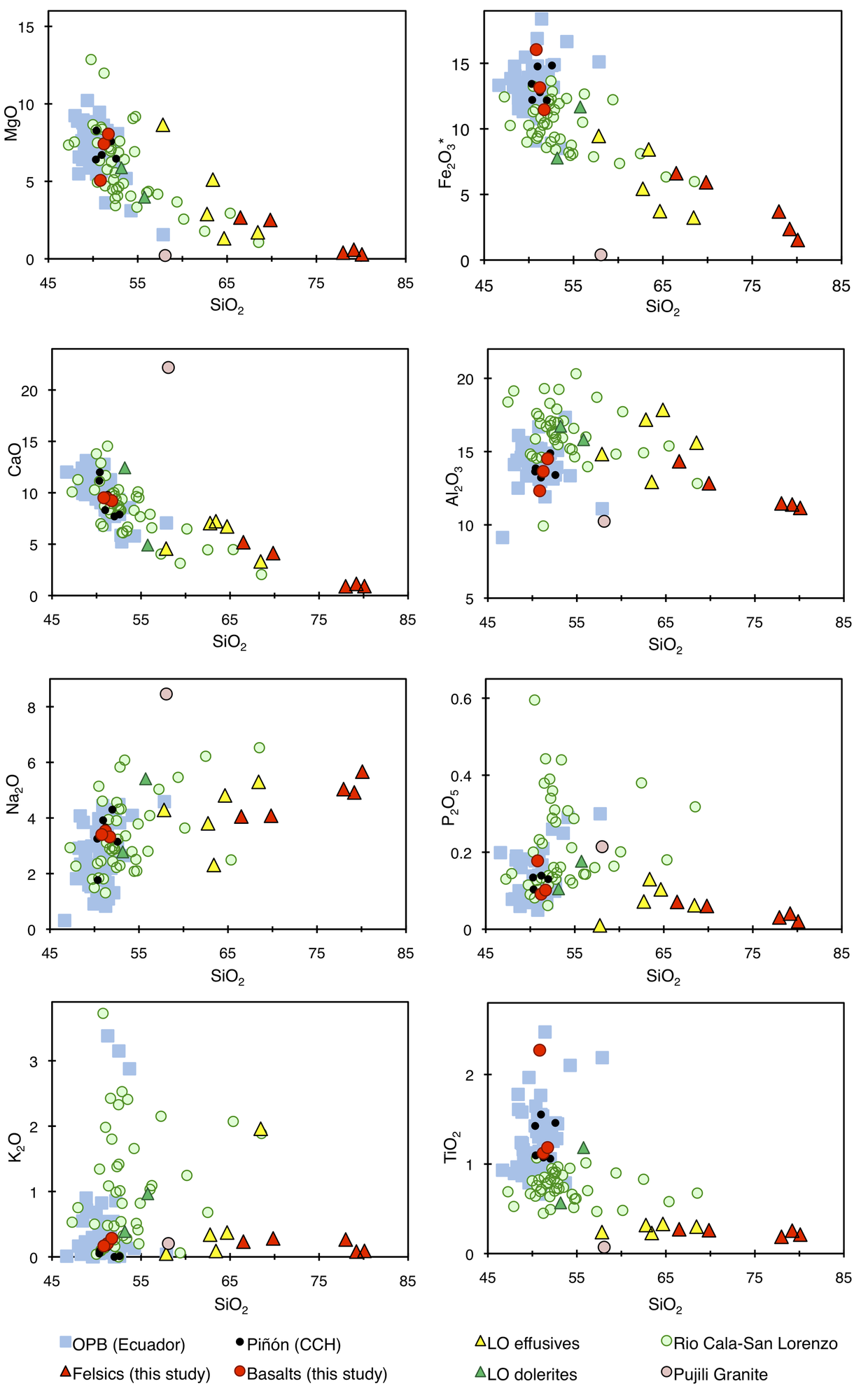
MgO
SiO2
Fe2O3*
CaO
Al2O3
Na2O
P2O5
K2O
TiO2
OPB (Ecuador)
Piñón (CCH)
LO effusives
Rio Cala-San Lorenzo
Felsics (this study)
Basalts (this study)
LO dolerites
Pujili Granite

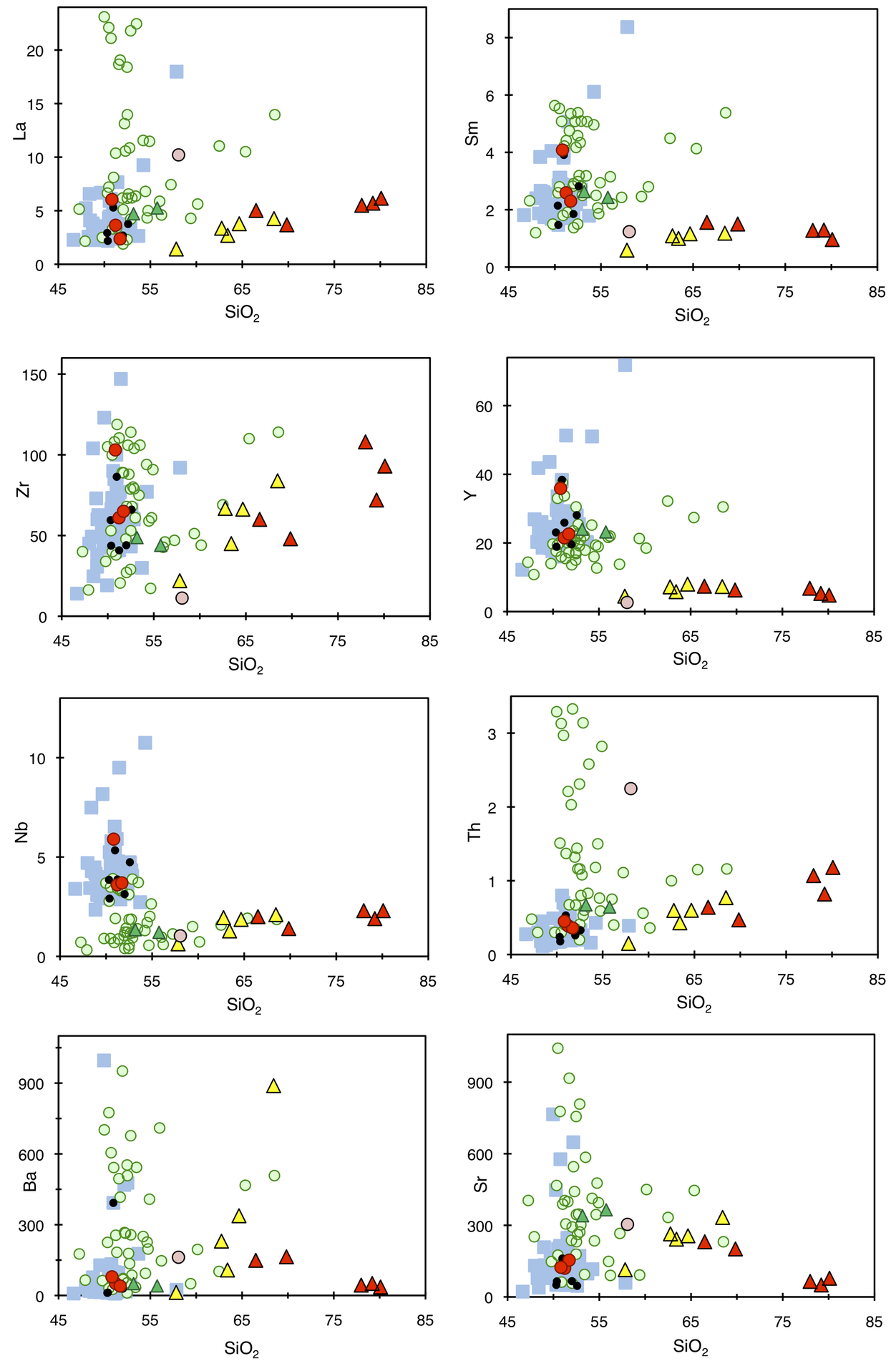
La
Sm
Zr
Y
Nb
Th
Ba
Sr
SiO2
OPB (Ecuador)
Piñón (CCH)
LO effusives
Rio Cala-San Lorenzo
Felsics (this study)
Basalts (this study)
LO dolerites
Pujili Granite

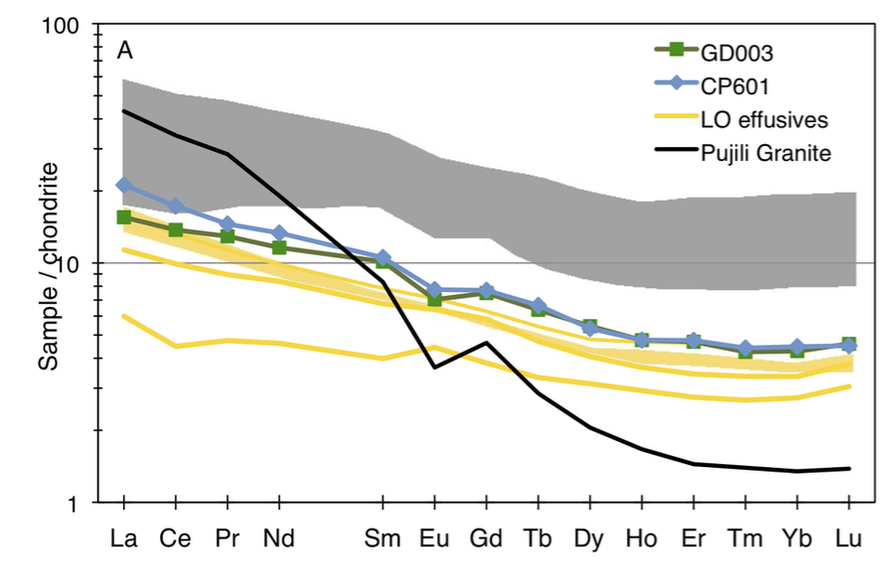
A
GD003
CP601
LO effusives
Pujili Granite
Sample / chondrite
100
10
1
La Ce Pr Nd Sm Eu Gd Tb Dy Ho Er Tm Yb Lu

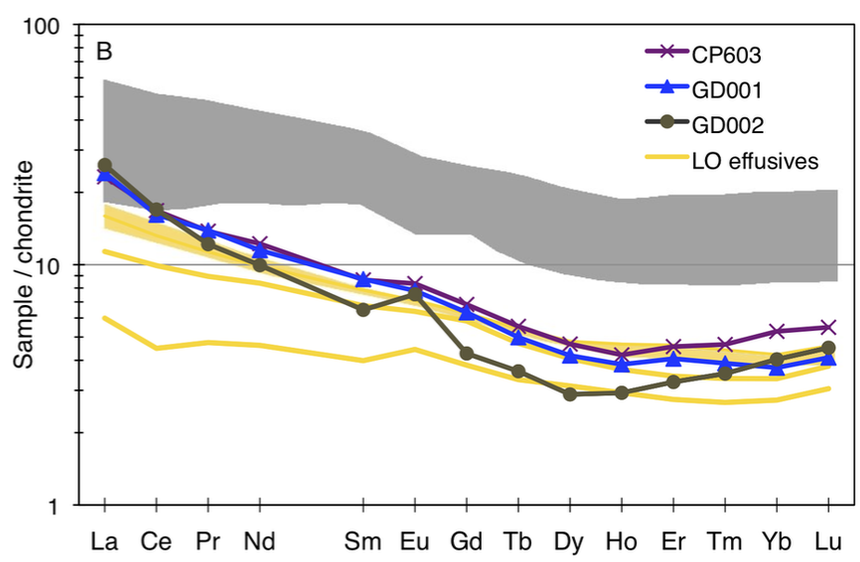
B
CP603
GD001
GD002
LO effusives
Sample / chondrite
100
10
1
La Ce Pr Nd Sm Eu Gd Tb Dy Ho Er Tm Yb Lu

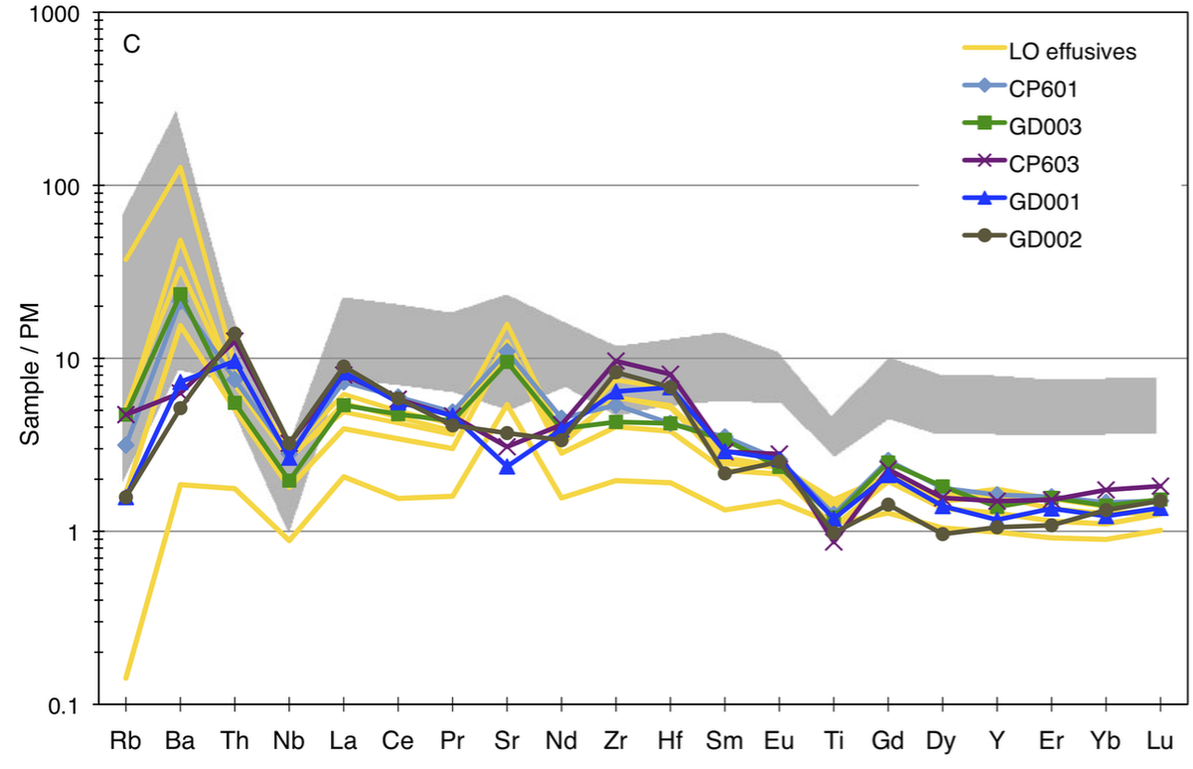
C
LO effusives
CP601
GD003
CP603
GD001
GD002
Sample / PM
1000
100
10
1
0.1
Rb Ba Th Nb La Ce Pr Sr Nd Zr Hf Sm Eu Ti Gd Dy Y Er Yb Lu

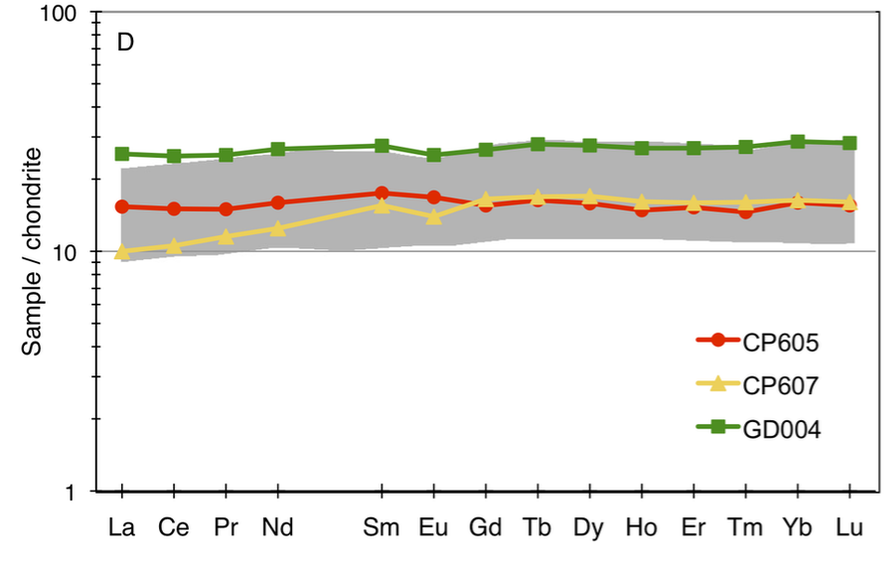
D
CP605
CP607
GD004
Sample / chondrite
100
10
1
La Ce Pr Nd Sm Eu Gd Tb Dy Ho Er Tm Yb Lu

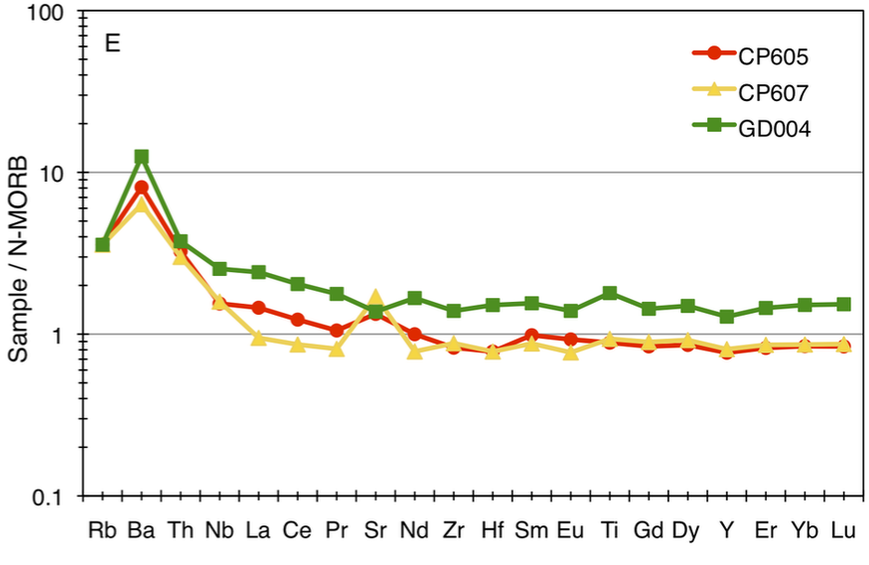
E
CP605
CP607
GD004
Sample / N-MORB
100
10
1
0.1
Rb Ba Th Nb La Ce Pr Sr Nd Zr Hf Sm Eu Ti Gd Dy Y Er Yb Lu

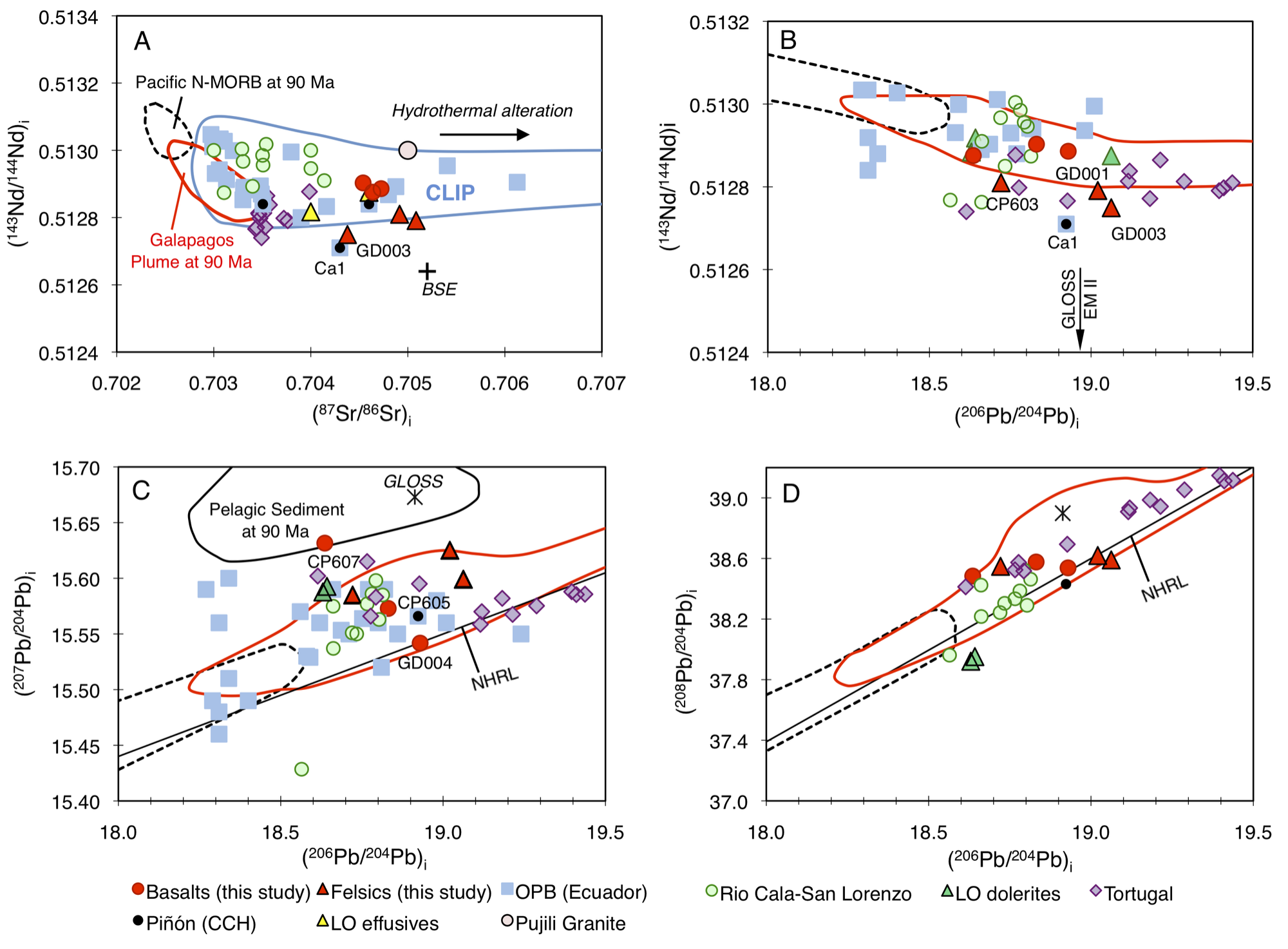
A
Pacific N-MORB at 90 Ma
Hydrothermal alteration
CLIP
Galapagos
Plume at 90 Ma
GD003
Ca1
BSE
0.5134
0.5132
0.5130
0.5128
0.5126
0.5124
0.702
0.703
0.704
0.705
0.706
0.707
(143Nd/144Nd)i
(87Sr/86Sr)i
B
GD001
CP603
Ca1
GD003
GLOSS
EM II
0.5132
0.5130
0.5128
0.5126
0.5124
18.0
18.5
19.0
19.5
(143Nd/144Nd)i
(206Pb/204Pb)i
C
GLOSS
Pelagic Sediment
at 90 Ma
CP607
CP605
GD004
NHRL
15.70
15.65
15.60
15.55
15.50
15.45
15.40
18.0
18.5
19.0
19.5
(207Pb/204Pb)i
(206Pb/204Pb)i
D
NHRL
39.0
38.6
38.2
37.8
37.4
37.0
18.0
18.5
19.0
19.5
(208Pb/204Pb)i
(206Pb/204Pb)i
Basalts (this study)
Felsics (this study)
OPB (Ecuador)
Rio Cala-San Lorenzo
LO dolerites
Tortugal
Piñón (CCH)
LO effusives
Pujili Granite

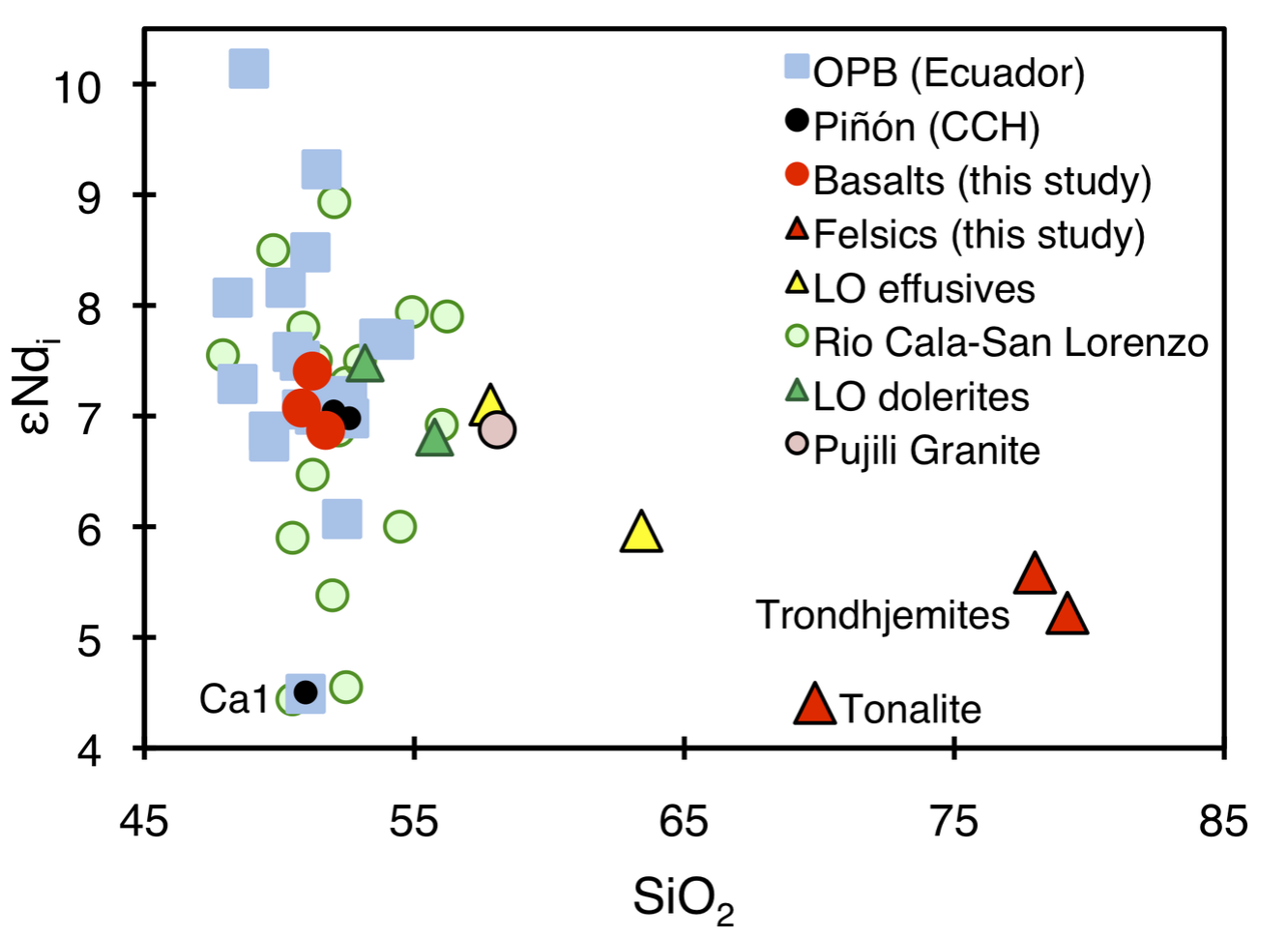
OPB (Ecuador)
Piñón (CCH)
Basalts (this study)
Felsics (this study)
LO effusives
Rio Cala-San Lorenzo
LO dolerites
Pujili Granite
Trondhjemites
Tonalite
Ca1
εNdi
SiO2
10
9
8
7
6
5
4
45
55
65
75
85

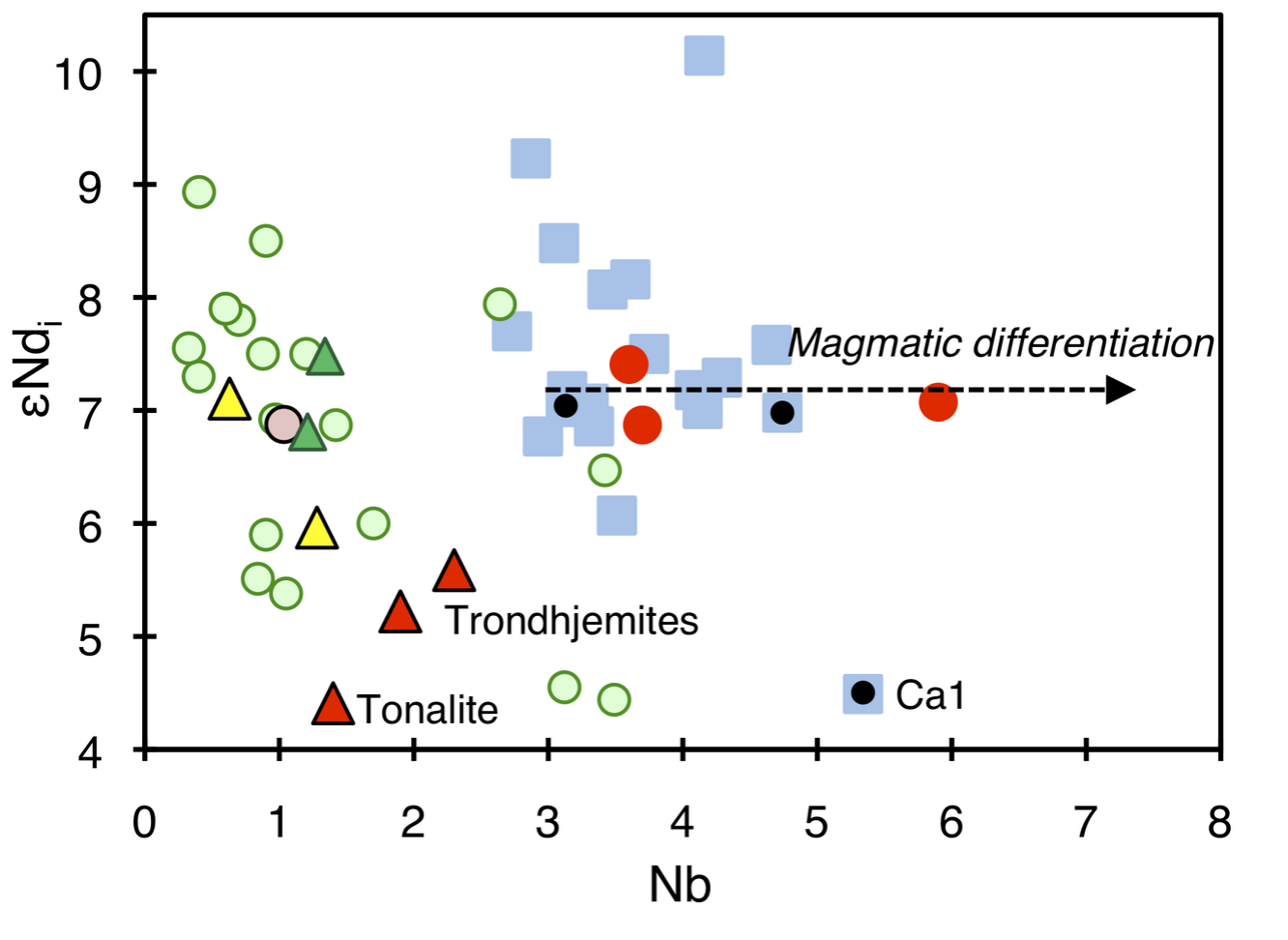
Magmatic differentiation
Trondhjemites
Tonalite
Ca1
εNdi
Nb
10
9
8
7
6
5
4
0
1
2
3
4
5
6
7
8

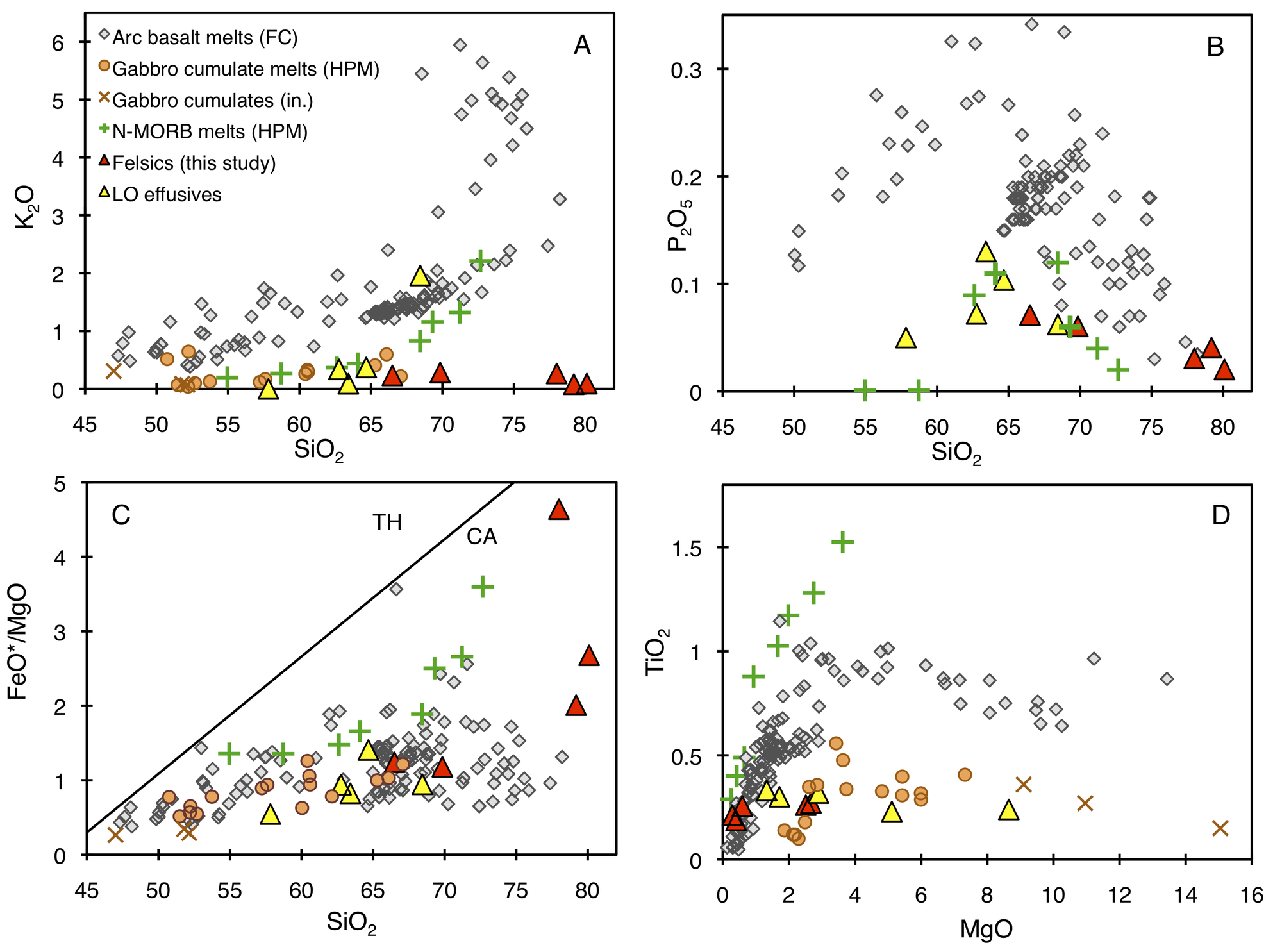
Arc basalt melts (FC)
Gabbro cumulate melts (HPM)
Gabbro cumulates (in.)
N-MORB melts (HPM)
Felsics (this study)
LO effusives
A
K2O
SiO2
B
P2O5
SiO2
C
TH
CA
FeO*/MgO
SiO2
D
TiO2
MgO